A Novel Differential Quadrature Galerkin Method for Dynamic and Stability Behaviour of Bi-directional Functionally Graded Porous Micro Beams

Ahmed Saimi*, Ismail Bensaid, Besma Khouani,
Med Yassin Mazari, Ihab Eddine Houalef
and Abdelmadjid Cheikh

IS2M Laboratory, Faculty of Technology, Mechanical Engineering Department, University Abou Bekr Belkaid, Tlemcen, Algeria
E-mail: ahmedsaimi@hotmail.fr
**Corresponding Author*

Received 30 June 2023; Accepted 30 September 2023;
Publication 03 November 2023

Abstract

The free vibration and buckling behaviours of 2D-FG porous microbeams are explored in this paper utilizing the Quasi-3D beam deformation theory based on the modified couple stress theory and a Differential Quadrature Galerkin Method (DQGM) systematically, as a combination of the Differential Quadrature Method (DQM) and the semi-analytical Galerkin method, which has used to reduce computational cost for problems in dynamics. The governing equations are obtained using the Lagrange's principle. The mass and stiffness matrices are calculated using the weighting coefficient matrices given by the differential quadrature (DQ) and Gauss-Lobatto quadrature rules. The matrices are expressed in a similar form to that of the Differential Quadrature Method by introducing an interpolation basis on the element boundary of the Galerkin method. The sampling points are determined by

European Journal of Computational Mechanics, Vol. 32_4, 393–440.
doi: 10.13052/ejcm2642-2085.3244

the Gauss-Lobatto node method. The influence of the thickness-to-material length scale parameter (MLSP) on the nondimensional natural frequencies and nondimensional critical buckling loads of 2D-FG porous microbeams are investigated, along with the effects of the boundary condition, aspect ratio and gradient index. The results are validated with literature to establish the accuracy of the procedure described. This work will provide a numerical basis for the design of FG microstructures in the field of micromechanics. These results can be applied to the engineering design of porous FG microstructures.

Keywords: DQGM, 2D-FG microbeam, porosity, couple stress, vibration and buckling.

1 Introduction

Rapid development of new material components has become necessary due to the expanding manufacturing demands in the aerospace, automotive and marine industries. By enlarging the range of the advanced materials that industrial scientists may create to satisfy the demands of mechanical characteristics such as enhanced stiffness and low density, etc. Researchers were attracted to the functionally graded materials (FGMs) to improve their performance and characteristics in the required directions as compared to conventional homogeneous materials. By adjusting the material characteristics of FGM during production, which will withstand exposure to severe environmental conditions, desired advanced mechanical properties may be attained. This is why industrialists and researchers are interested in examining how FGM construction functions when considering static, buckling and dynamic loads.

As it is known in structural engineering, most of structural components such as beams, plates and shells are generally thick and the presence of shear deformations is unavoidable. Researchers frequently refer to the first-order shear deformable beam theory (FSBT), higher-order shear deformable beam theory (HSBT), and shear and normal deformable beam theory also known as quasi-3D theory are well-used by researchers. The FSBT is the most straightforward model, but it requires a shear correction factor since it does not satisfy the zero traction boundary criteria at the top and bottom surfaces of the beam [1, 2]. As a result, the HSBT theories were proposed, which improved the transverse shear stress distribution and consequently eliminating the requirement for a shear correction factor (SCF) [3]. However, the normal strain or stretch effects which becomes very important and

should be considered for thick typical FGBs, is not taken into account by HSBT theories. As a result, quasi-3D theories [4, 5] that consider the shear and stretching effects are generated using the assumption of higher order variation of both axial and transverse displacements. Conventional FGBs (or 1D-FGBs) designed by varying material characteristics just in one direction sometimes may not meet necessary requirements, such as the temperature, hygrothermal and stress distributions in two or three directions for specific advanced construction such aircraft vehicles and shuttles [6]. To address this shortcoming of the traditional FGBs, researchers have recently focused their attention on a novel type of FGB with material properties that vary in two or three dimensions. In [7], a method based on the Element Free Galerkin method is provided for the simulation and optimization of the vibration response of bidirectional functionally graded beams. Semi-analytical elasticity solutions for the bending and thermal deformations of BDFGBs with varying end conditions are obtained by employing the state-space based differential quadrature approach in [8]. [9] investigated the flexure behaviour of the two directions FG sandwich beams using a quasi-3D theory and a Meshless approach. [10] explored the vibrational responses of 2D-FG Timoshenko beams excited by a moving concentrated load based on combination between finite element and Newmark method. Using the Galerkin approach, the bending vibration of bi-directionally exponentially orthotropic plates supported on the Pasternak elastic foundation were inspected by [11]. More recently, [12] studied the effect of variable axial loads (VALs) on the maximum frequencies and buckling loads of bi-directional functionally graded beam. The beam was modelled by Reddy type higher shear deformation model and Ritz procedure was used to solve the system of governing equations related to the provided problem. [13] this paper proposes a new nonlocal higher-order hyperbolic shear deformation beam theory (HSBT) for the static bending and vibration of nanoscale-beams. [14] in this article, static deflection and buckling of functionally graded (FG) nanoscale beams made of porous material are carried out based on the nonlocal Timoshenko beam model which captures the small scale influences. [15] forced vibration analysis of a cracked functionally graded microbeam is investigated by using modified couple stress theory with damping effect. [16] in this study, static bending of an edge cracked cantilever nanobeam composed of functionally graded material (FGM) subjected to transversal point load at the free end of the beam is investigated based on modified couple stress theory. [17] in this work, dynamic behaviour of functionally graded (FG) porous nano-beams is studied based on nonlocal nth-order shear deformation theory which takes

into the effect of shear deformation without considering shear correction factors. [18] the bending, stability (buckling) and vibration response of nano sized beams is presented in this study based on the Eringen's nonlocal elasticity theory in conjunction with the Euler-Bernoulli beam theory. [19] this paper presents a new nonlocal Hyperbolic Shear Deformation Beam Theory (HSDBT) for the free vibration of porous Functionally Graded (FG) nanobeams. [20] this study explores the linear and nonlinear solutions of sigmoid functionally graded material (S-FGM) nanoplate with porous effects. [21] this paper presents sets of explicit analytical equations that compute the static displacements of nanobeams by adopting the nonlocal elasticity theory of Eringen within the framework of Euler Bernoulli and Timoshenko beam theories. [22] investigated the dynamic and buckling response of bidirectional graded material beams (BDFB) with transverse cracks. [23] this work explores the free vibratory behaviour of imperfect BD-FG microbeams with a crack using the Quasi-3D shear and normal deformation beam concept, MCST, and DQFEM. [24] the study aims to investigate the dynamic response of a tapered rotor shaft system made of ceramic-metal materials using the differential quadrature finite elements method (DQFEM). The purpose of the investigation is to identify natural frequencies for modelling and analysis of the structure. [25] employs the h-p hybrid finite element method to perform dynamic analysis of a symmetrical on-board rotor on mobile dimensionally stable supports.

Recently, materials with a porous structure have attracted the attention of several researchers because of their special mechanical characteristics. The presence of porosity can affect the functionally graded materials and have a great advantage like good protection from temperature, good insulation of sound and a very good absorption of energy and electromagnetic waves. In the literature, one can find various researches on porous structures. Among the first works in this field, we find the works of [26], who worked on the impact of the presence of porosities in functionally graded materials realized by a process of sequential infiltration in several stages. They determined that it is important to consider the porosity effect when designing and studying the behaviour of FGM structures. In another study, [27] investigated the nonlinear and linear dynamic responses of FGM beams made of porous materials and taking in consideration the fixed boundary supports. [28] presented an analysis on the buckling of a circular shaped plate made of porous metallic foam material. [29] made a study on the elastic buckling and the static bending of porous beams made of metal foam via the theory of Timoshenko's beam. In their work [30], they also studied the non-linear free vibrations of a

porous foam metal sandwich beam. [31] did a work on the free vibration of thick rectangular plates made of porous metal foam using the unified Carrera formulation. [32] examined the post-buckling behaviour of metal foam nanobeams with imperfect geometry. [14] investigated the static deflection and buckling of functionally graded (FG) nanoscale beams in porous material and are made based on the nonlocal Timoshenko beam model that captures small-scale influences. [33] investigated the stability and dynamic behaviour of porous cell plates with uniform and non-uniform porosity variations using first-order shear deformation theory. [34] investigated the thermomechanical performance of porous FG beams subjected to various thermal loads with two distinct porosity distributions using the improved four-variable shear-strain beam theory. With new technological advancements, extreme requirements based on the use of micro/nano electromechanical systems (MEMS/NEMS) such as actuators, thin films, sensors, probes, etc. have been raised by different industries [35]. However, experiments indicate that the mechanical behaviour of micro/nano elements cannot be studied by classical continuum theories (CCT), due to their limitations in capturing the scaling effect. More reliable prediction can be obtained using higher order continuum theories (HOCT) in which additional hardware parameters and scales are required [36]. In order to study the size effect in micro and nano structures, in the literature, several have proposed non-classical theories of continuum mechanics. Among these theories is the work of [37] who presented a high order non-local strain-gradient and elasticity theory that take in to account high order stress gradients and the non -locality of the deformation gradient. The theory of strain gradient elasticity was introduced by the work of [38], hence the density of potential energy depends on the first and second gradients of the deformation. [39] made an observation on the effect of the size of the structure when it is reduced to the micro/nano scale, from the experimental results, which allowed the application of the order equilibrium conditions to strain gradient elasticity theory and the number of independent elastic length scale parameters is reduced from five to three, [39] suggested a Modified Stress Gradient Theory (MSGT), from which a new upper-order measurements were used to characterise stress gradient behaviours. This theory proposes that the strain energy density is dependent on the symmetric strain, deviatoric stretch gradient and symmetric rotation gradient tensors, and also the dilation gradient vector. Within the framework of the modified deformation gradient theory, several researchers have studied the behaviours of vibration, buckling and bending of micro-structures, such as [40–43]. In the scientific research literature, some researchers have studied

the mechanical characteristics of microbeams. For example, [44] analysed free vibration and static bending of microbeams with functional gradient material using modified torque stress theory and the theory of higher order beam. Based on theory of amended torque stress, the effect of temperature on the free vibrations and the buckling of microbeams has been treated by [45]. Using the theory of non-local elasticity and the theory of Timoshenko's beam, [46] have investigated the bending of isotropic microbeams. furthermore [47] analysed a porous microbeam model for vibration analysis based on modified stress gradient theory and sinusoidal beam theory via the method Analytics from Navier's. Most of the above works have used analytical or experimental methods in their studies. And also, some have used numerical methods such as the generalized differential quadrature method [48]. There is also the work of [49] who investigate free vibration analysis of functionally graded porous microplates with shear and normal deformation via the classical finite element method. [50] investigated the vibrational and critical circular speed characteristics of a functionally graded (FG) rotary micro-disk using a non-local continuum model called the modified couple stress (MCS) model. For deriving and solving non-classical final relations, the generalized differential quadrature (GDQ) approach and variational method are used. [51] studied the stability of cantilevered curved microtubules in axons using various size elements and the generalized differential quadrature method to solve equations. Recently a new combination between the hierarchical finite element method and the generalized differential quadrature method was applied for the study of the dynamic response of an onboard rotor [52], this method was used for the first time in the work of [53] for the applications to vibrations and bending of Mindlin plates with curvilinear domains. [54] presented a dynamic finite elements procedure capable of analysing the dynamic behaviour of perforated Timoshenko microbeams in thermal environment and subjected to moving mass for the first time. [55] investigated the behaviour of the nonlinear flexural free vibration micro beams with reinforcement of graphene platelets via the classical finite element method coupled with trigonometric shear flexible beam model. [56] investigated a comparative study of various formulations with a weak form of quadrature element method. [57] used a quasi-3D theory for free vibration analysis of FG microbeams to investigate the effect of porosity distribution form. Based on the uneven porosity distribution of the porous FG materials, [49] used the classical finite element approach to investigate the size-dependent natural frequencies of functional gradient shear (FG) and normal deformable porous square microplates. [58] examined the size-dependent free vibration of porous nanoplates resting on a Kerr

foundation in a hygrothermal environment. The material properties of functionally graded (FG) porous nanoplates are supposed to change continuously in the thickness direction, with three different porosity patterns, according to the modified power-law model. [59] combined a classical finite element method and the transverse shear-normal deformable beam theory (TSNDBT) for the dynamics and stability analysis of bidirectional FG microbeam with 2D porosity and variable material length scale. [60] studied the vibration behaviour of 2D-FG nano and microbeams made of porous materials, via the generalized differential quadrature method (GDQM) based on Timoshenko beam. [61] studied the buckling behaviour of 2D-FG nano and microbeams made of porous materials, via the generalized differential quadrature method (GDQM) based on Euler Bernoulli beam.

What can be seen from the works cited above and others existing in the literature is that studies on beams in graded materials are the basis of numerical resolution methods such as finite element, isogeometric, DQM and analytical like Ritz and Navier method with limitations. Furthermore, no research has been conducted in the literature yet that involves the free vibration analysis of BDFG microbeams by using a semi-numerical procedure to solve the governing equations of motions more efficiently, such as the named Differential Quadrature Galerkin method (DQGM), which combines the efficiency of quadrature for integration and calculation speed and the semi-analytical part which provides the precision of the obtained results and the variable boundary conditions. Hence, this paper is devoted to investigating the free vibration and buckling responses of bi-directional FG porous microbeams in combination with quasi-3D beam theory by employing a robust semi-analytical procedure named Differential Quadrature Galerkin Method (DQGM) as a combination of the Differential Quadrature Method (DQM) and the semi-analytical Galerkin method, which has used to reduce computational cost for problems in engineering design. The material characteristics of the FG beam change according to a power law along both thickness and axial axes. The Lagrange's principle is used to generate the governing equations. The mass, geometric and stiffness matrices are calculated using the weighting coefficient matrices given by the differential quadrature (DQ) and Gauss-Lobatto quadrature rules. The matrices are expressed in a similar form to that of the Differential Quadrature Method by introducing an interpolation basis on the element boundary of the Galerkin method. The sampling points are determined by the Gauss-Lobatto node method. The collected results are compared to the existing results in the literature to check the accuracy of the presented method. The influence of FG beam material gradient indices,

length to thickness ratios, boundary conditions, and other characteristics on the frequency and buckling load of BDFG beams are thoroughly examined and analysed.

2 Formulation and Theories

2.1 Model of Porous 2D-FG Microbeam

In this work, we consider a bidirectionally porous functionally graded material micro-beam with the following geometric properties: a length *L*, a width *b*, and a thickness *h*, as shown in Figure 1.

Assume that the FG porous microbeam is composed of a mixture of metal on the bottom surface $z = -h/2$, and ceramic on the top surface $z = h/2$. Moreover, the material parameters are assumed to vary continuously along the thickness and length directions. It also includes the influence of porosities in the production process of functionally graded porous materials. The porosity distribution in the FG microbeam is assumed across the thickness direction, according to the porosity with even distribution. The distributions of the material properties of the FG porous microbeam take the form according to the following equations:

$$\text{solide FGM: } P(z) = (P_c - P_m)\left(\frac{z}{h} + \frac{1}{2}\right)^{k_z}\left(\frac{x}{L}\right)^{k_x} + P_m \tag{1}$$

$$\text{Even: } P(z) = (P_c - P_m)\left(\frac{z}{h} + \frac{1}{2}\right)^{k_z}\left(\frac{x}{L}\right)^{k_x} + P_m - \frac{\alpha_0}{2}(P_c + P_m) \tag{2}$$

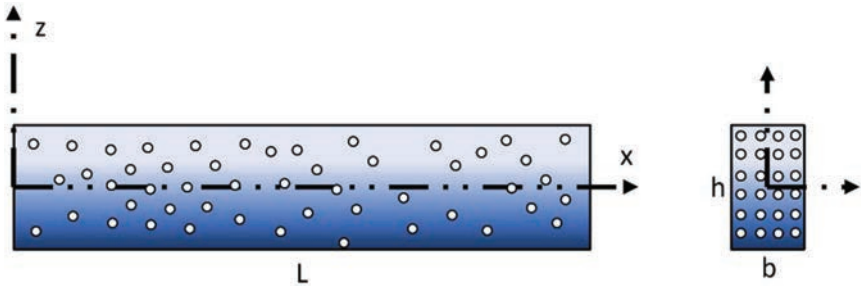

Figure 1 Geometry of porous bidirectional FG microbeam.

Where P_m, P_c, indicate materials properties such as the young's modulus, mass density, Poisson's ratio, and VMLSP. The indices *c* and *m* indicate ceramic and metal respectively. $k_z,\ k_x$ are the power-law volume fraction index that defines the FG material variation characterization through the thickness and the length of the microbeam. The coefficient $\alpha_0(\alpha_0 \leq 1)$ is the volume fraction of the porosity distribution to determine the porosity void size.

2.2 Strain Gradient Elasticity Theory

According to the Modified Couple Stress Theory (MCST) of [62], the strain, kinetic, and potential energies will be employed to develop the governing equations of the porous microbeam:

$$U = \frac{1}{2}\int_0^L \int_A (\sigma_{ij}\varepsilon_{ij} + m_{ij}^s \chi_{ij}^s) dA dx \tag{3}$$

Hence ε_{ij}, and χ_{ij}^s represents respectively the strain tensor, and the rotationally symmetric gradient tensor which are defined by the following equations, a subscripted comma is used to denote the derivative with respect to the followed variable.

$$\varepsilon_{ij} = \frac{1}{2}(u_{i,j} + u_{j,i}) \tag{4}$$

$$\chi_{ij}^s = \frac{1}{2}(\theta_{i,j} + \theta_{j,i}) \tag{5}$$

$$\theta_i = \frac{1}{2} e_{ijk} u_{k,j} \tag{6}$$

Where u_i, θ_i are the components of displacement vector, the components of rotation vectors, the Kronecker delta and the permutation symbols, respectively.

$$\sigma_{ij} = \lambda \varepsilon_{mm} \delta_{ij} + 2\mu \varepsilon_{ij} \tag{7}$$

$$m_{ij}^s = 2\mu l_2^2 \chi_{ij}^s \tag{8}$$

σ is are the classical stress tensor, and m^s is the higher order strain tensors.

The independent parameters of symmetrical rotational gradients-related material length scale are represented by l.

$$\mu = \frac{E}{2(1+\nu)} \tag{9}$$

$$\lambda = \frac{E\nu}{(1-\nu^2)} \tag{10}$$

Hence μ and λ are the Lame constants, and ν is the Poisson's ratio.

2.3 Kinematics Formulation

Based on a Quasi-3D beam theory, the displacement field at any arbitrary location on the microbeam is assumed to be stated as follows in the current work [63]:

$$\begin{cases} u_1(x,z,t) = u(x,t) - z\dfrac{dw_b}{dx} + f_1(z)\dfrac{dw_s}{dx} \\ u_2(x,z,t) = 0 \\ u_3(x,z,t) = w_b(x,t) + w_s(x,t) + f_2(z)w_z(x,t) \end{cases} \tag{11}$$

According to this theory, the transverse displacement is divided into three parts w_b, w_s and w_z.

Where u, w_b, w_s and w_z are respectively, the displacement in the plane in the directions $x-$, the bending, shear and normal components of the transverse displacement of the points on the neutral axis of the beam. Our choice of functions is determined based on shear function given by Reddy Equation (12) knowing that $f_2(z) = 1 + \frac{df_1}{dz}(z)$:

$$f_1(z) = -\frac{4z^3}{3h^3} \tag{12}$$

By introducing Equation (11) into Equation (4), we obtain the non-zero deformation torsor components:

$$\begin{cases} \varepsilon_{11} = \dfrac{du}{dx} - z\dfrac{d^2w_b}{dx^2} + f_1\dfrac{d^2w_s}{dx^2} \\ \varepsilon_{33} = \dfrac{df_2}{dz}w_z \\ \gamma_{13} = \left(1 + \dfrac{df_1}{dz}\right)\dfrac{dw_s}{dx} + f_2\dfrac{dw_z}{dx} \end{cases} \tag{13}$$

By replacing Equation (13) in (7) we obtain the strain tensor:

$$\begin{cases} \sigma_{11} = \left(\dfrac{E}{1-\nu^2}\right)\varepsilon_{11} + \left(\dfrac{E\nu}{1-\nu^2}\right)\varepsilon_{33} \\ \sigma_{13} = \left(\dfrac{E}{1-\nu^2}\right)\left(\dfrac{1-\nu}{2}\right)\gamma_{13} \\ \sigma_{33} = \left(\dfrac{E\nu}{1-\nu^2}\right)\varepsilon_{11} + \left(\dfrac{E}{1-\nu^2}\right)\varepsilon_{33} \end{cases} \tag{14}$$

Introducing Equation (11) into (6) gives:

$$\begin{cases} \theta_1 = 0 \\ \theta_2 = \dfrac{1}{2}\left(-2\dfrac{dw_b}{dx} - \left(1 - \dfrac{df_1}{dz}\right)\dfrac{dw_s}{dx} - f_2\dfrac{dw_z}{dx}\right) \\ \theta_3 = 0 \end{cases} \tag{15}$$

The components non-zero of rotationally symmetrical gradient tensor χ^s are obtained by replacing Equation (15) in Equation (5):

$$\begin{cases} \chi^s_{23} = \chi^s_{32} = \dfrac{1}{4}\left(\dfrac{d^2 f_1}{dz^2}\dfrac{dw_s}{dx} - \dfrac{df_2}{dz}\dfrac{dw_z}{dx}\right) \\ \chi^s_{12} = \chi^s_{21} = \dfrac{1}{4}\left(-2\dfrac{d^2 w_b}{dx^2} - \left(1 - \dfrac{df_1}{dz}\right)\dfrac{d^2 w_s}{dx^2} - f_2\dfrac{d^2 w_z}{dx^2}\right) \end{cases} \tag{16}$$

Replacing Equation (16) in Equation (8) gives the non-zero higher order constraints m^s_{ij} such as:

$$\begin{cases} m^s_{23} = m^s_{32} = \dfrac{E}{(1+\nu)}{l_2}^2\chi^s_{23} \\ m^s_{12} = m^s_{21} = \dfrac{E}{(1+\nu)}{l_2}^2\chi^s_{12} \end{cases} \tag{17}$$

The substitution of Equations (11)–(17) in Equation (3):

$$U = \frac{1}{2}\int_0^L \left(J_1\left(\frac{du}{dx}\right)^2 - 2J_2\frac{du}{dx}\frac{d^2 w_b}{dx^2} + 2J_3\frac{du}{dx}\frac{d^2 w_s}{dx^2}\right.$$
$$\left. - 2J_4\frac{d^2 w_b}{dx^2}\frac{d^2 w_s}{dx^2} + J_5\left(\frac{d^2 w_b}{dx^2}\right)^2 + J_6\left(\frac{d^2 w_s}{dx^2}\right)^2\right.$$

$$
\begin{aligned}
&+ J_7 {w_z}^2 + 2J_8 \frac{du}{dx} w_z - 2J_9 \frac{d^2 w_b}{dx^2} w_z + 2J_9 \frac{d^2 w_s}{dx^2} w_z \\
&+ J_{11} \left(\frac{dw_s}{dx} \right)^2 + 2J_{12} \frac{dw_s}{dx} \frac{dw_z}{dx} + J_{13} \left(\frac{dw_z}{dx} \right)^2 \\
&+ \frac{1}{2} J_{14} \left(\frac{d^2 w_b}{dx^2} \right)^2 + \frac{1}{2} J_{15} \frac{d^2 w_b}{dx^2} \frac{d^2 w_s}{dx^2} + \frac{1}{8} J_{16} \left(\frac{d^2 w_s}{dx^2} \right)^2 \\
&+ \frac{1}{4} J_{17} \frac{d^2 w_s}{dx^2} \frac{d^2 w_z}{dx^2} + \frac{1}{2} J_{18} \frac{d^2 w_b}{dx^2} \frac{d^2 w_z}{dx^2} + \frac{1}{8} J_{19} \left(\frac{d^2 w_z}{dx^2} \right)^2 \\
&+ \frac{1}{8} J_{20} \left(\frac{dw_s}{dx} \right)^2 + \frac{1}{8} J_{21} \left(\frac{dw_z}{dx} \right)^2 - \frac{1}{4} J_{22} \frac{dw_s}{dx} \frac{dw_z}{dx} \Bigg) dx
\end{aligned} \tag{18}
$$

With:

$$
\begin{cases}
\{I_{1:7}\} = b \displaystyle\int_{-\frac{h}{2}}^{\frac{h}{2}} \left(\frac{E}{1-\nu^2} \right) \left(1, z, f_1, z f_1, z^2, {f_1}^2, \left(\frac{df_2}{dz} \right)^2 \right) dz \\
\{I_{8:10}\} = b \displaystyle\int_{-\frac{h}{2}}^{\frac{h}{2}} \left(\frac{E\nu}{1-\nu^2} \right) \frac{df_2}{dz} (1, z, f_1) dz \\
\{I_{11:13}\} = b \displaystyle\int_{-\frac{h}{2}}^{\frac{h}{2}} \left(\frac{E}{2(1+\nu)} \right) \left(\left(1 + \frac{df_1}{dz} \right)^2, f_2 \left(1 + \frac{df_1}{dz} \right), {f_2}^2 \right) dz \\
\{J_{14:22}\} = b \displaystyle\int_{-\frac{h}{2}}^{\frac{h}{2}} \left(\frac{E}{(1+\nu)} l^2 \left(1, \left(1 - \frac{df_1}{dz} \right), \left(1 - \frac{df_1}{dz} \right)^2, \right. \right. \\
\qquad f_2 \left(1 - \frac{df_1}{dz} \right), f_2, {f_2}^2, \left(\frac{d^2 f_1}{dz^2} \right)^2, \\
\qquad \left. \left. \left(\frac{df_2}{dz} \right)^2, \frac{d^2 f_1}{dz^2} \frac{df_2}{dz} \right) \right) dz
\end{cases} \tag{19}
$$

The potential energy is given as follow:

$$
V = -\frac{1}{2} \int_0^L N_0 \left[\left(\frac{dw_b}{dx} \right)^2 + \left(\frac{dw_s}{dx} \right)^2 + 2 \frac{dw_b}{dx} \frac{dw_s}{dx} \right] dx \tag{20}
$$

The Kinetic Energy can be written as:

$$T = \frac{1}{2}\int_0^l \int_A \rho[\dot{u}_1^2 + \dot{u}_2^2 + \dot{u}_3^2]dAdx \tag{21}$$

By replacing Equation (11) in Equation (21) we obtain the final form of the kinetic energy:

$$\begin{aligned} T = \frac{1}{2}\int_0^l \Bigg[& J_1(\dot{u}^2 + \dot{w}_b^2 + \dot{w}_s^2 + 2\dot{w}_b\dot{w}_s) - 2J_2\dot{u}\frac{d\dot{w}_b}{dx} + 2J_3\dot{u}\frac{d\dot{w}_s}{dx} \\ & - 2J_4\frac{d\dot{w}_b}{dx}\frac{d\dot{w}_s}{dx} + J_5\left(\frac{d\dot{w}_b}{dx}\right)^2 + J_6\left(\frac{d\dot{w}_s}{dx}\right)^2 \\ & + J_7\dot{w}_z^2 + 2J_8(\dot{w}_b\dot{w}_z + \dot{w}_s\dot{w}_z)\Bigg]dx \end{aligned} \tag{22}$$

Hence the mass moments of inertia are given by:

$$\begin{aligned} & \{J_1, J_2, J_3, J_4, J_5, J_6, J_7, J_8\} \\ & \quad = b\int_{-\frac{h}{2}}^{\frac{h}{2}} \rho(1, z, f_1, zf_1, z^2, {f_1}^2, {f_2}^2, f_2)dz \end{aligned} \tag{23}$$

2.4 Differential Quadrature Galerkin Formulation

The derivative of a function at a point is approximated by a weighted linear sum of field variables along a line through the spot using established DQ criteria. Any other complete basis, besides to Lagrange functions, can be utilized to formulate DQ rules [52, 64, 65].

As a result, the order n derivative of a field variable $g(x)$ at a discrete location x_i can be represented as:

$$\left.\frac{\partial^n g(x,t)}{\partial x^n}\right|_{x_i} = \sum_{j=1}^{N} A_{ij}^{(n)} g(x_j, t) \quad (i = 1, 2, 3, \ldots, N) \tag{24}$$

With $A_{ij}^{(n)}$ is the weighting coefficient related to the derivative of order n, and the weighting coefficient is obtained by the following.

If $n = 1$, then

$$\begin{aligned} A_{ij}^{(1)} &= \frac{M(x_i)}{(x_i - x_j)M(x_j)} \quad i \neq j,\ i, j = 1, 2, \ldots, N \\ A_{ii}^{(1)} &= -\sum_{j=1, j\neq i}^{n} A_{ij}^{(1)} \qquad i = 1, 2, \ldots, N \end{aligned} \tag{25}$$

With

$$\begin{aligned} M(x_i) &= \prod_{k=1, k\neq i}^{N} (x_i - x_k) \\ M(x_j) &= \prod_{k=1, k\neq i}^{N} (x_j - x_k) \end{aligned} \tag{26}$$

If $n > 1$, the second and higher order derivatives, the weighting coefficients are determined using the following simple recurrence relation:

$$\begin{aligned} A_{ij}^{(n)} &= n\left(A_{ij}^{(1)} * A_{ii}^{(n-1)} - \frac{A_{ij}^{(n-1)}}{(x_i - x_j)}\right) \quad i \neq j,\ i, j = 1, 2, \ldots, N,\ n > 1 \\ A_{ii}^{(n)} &= -\sum_{j=1, j\neq i}^{N} A_{ij}^{(n)} \qquad\qquad\qquad\qquad i = 1, 2, \ldots, N \end{aligned} \tag{27}$$

The Gauss-Lobatto quadrature rules theory can be found in the mathematical literature; The Gauss-Lobatto quadrature rule with a degree of accuracy. $(2n - 3)$ for the function $g(x)$ defined in $[-1, 1]$ is:

$$\int_{-1}^{1} f(x)dx = \sum_{j=1}^{N} C_j g(x_j) \tag{28}$$

With the weighting coefficient C_j of the Gauss-Lobatto integration is given by:

$$C_1 = C_N = \frac{2}{N(N-1)}, \quad C_j = \frac{2}{N(N-1)[P_{N-1}(x_j)]^2} \quad (j \neq 1, N) \tag{29}$$

x_j is the $(j-1)$ zero of the first order derivative of $P_{N-1}(x)$. We will utilize the recursion formula as Equations (30) and (31) to solve the roots of Legendre polynomials; it is simple to find thousands of roots this way.

$$P_{N+1}(x) = \frac{2N+1}{N+1} x P_N(x) - \frac{N}{N+1} P_{N-1}(x) \tag{30}$$

With $P_0(x) = 1$, $P_1(x) = x$. The n-order derivation of Legendre polynomials can be determined by the following equation:

$$P_{N+1}^{(n)}(x) = x P_N^{(n)}(x) + (N+n) P_N^{(n)}(x) \tag{31}$$

In order to obtain a denser population near the boundaries, the sample points are selected according to the Gauss-Lobatto grid distribution of nodes.

$$x_j = -\cos\left(\frac{j-1}{N-1}\pi\right) \tag{32}$$

The Gauss-Lobatto nodes are solved with the Newton-Raphson iteration method.

$$x^{iT+1} = x^{iT} - \boldsymbol{F}'(x^{iT})^{-1} \boldsymbol{F}(x^{iT}), \quad iT = 0, 1, \ldots \tag{33}$$

$$x = [x_2, x_3, \ldots, x_{N-1}]^T \tag{34}$$

$$\boldsymbol{F}(x) = [f(x_2), f(x_3), \ldots, f(x_{N-1})]^T \tag{35}$$

$$\boldsymbol{F}'(x) = \left[\frac{\partial f(x_j)}{\partial x_i}\right]_{(N-2)\times(N-2)} \tag{36}$$

$$f(x_j) = \sum_{k-1,\ k\neq j}^{N} \frac{1}{x_j - x_k} \quad j = 2, 3, \ldots, N-1 \tag{37}$$

$$\frac{\partial f(x_j)}{\partial x_i} = \begin{cases} -\sum\limits_{k=1,\ k\neq j}^{N} \dfrac{1}{(x_j - x_k)^2}, & (i = j) \\ \dfrac{1}{(x_j - x_i)^2}, & (i \neq j) \end{cases} \tag{38}$$

The value of x at the iT^{th} iteration step is denoted by *k*. This approach is less affected by the starting value. As beginning values, the values given by Equation (32) are employed.

In this section we aim to illustrate the use of DQGM through the microbeam.

According to the Galerkin method, the displacement functions $u(x,t)$, $w_{b,s,z}(x,t)$ are assumed respecting the boundary conditions as follows:

$$\begin{cases} u[x(\xi)] = \sum_{m=1}^{N} \left[U_m \dfrac{dX_m}{dt} \right] e^{j\omega t} \\ w_b[x(\xi)] = \sum_{m=1}^{N} [B_m X_m] e^{j\omega t} \\ w_s[x(\xi)] = \sum_{m=1}^{N} [S_m X_m] e^{j\omega t} \\ w_z[x(\xi)] = \sum_{m=1}^{N} [Z_m X_m] e^{j\omega t} \end{cases} \tag{39}$$

With X_m is the shape functions at m mode as given by Equation (40). The number N of sampling points is equal to m maximum number of shape modes. Where r, p, and q are index coefficients for different boundary conditions BCs. The values of r, p, and q are given for each boundary condition by Table 1.

$$X_m = (-1)^r \sin^{(p+1)} \left(m\pi \frac{x(\xi)}{L} \right) \left(\cos \left((2m - r) i\pi \frac{x(\xi)}{2L} \right) - 1 \right)^q \tag{40}$$

The local coordinates are related to the dimensionless coordinates by the relation:

$$x = \frac{L_e}{2}(\xi + 1) \; avec - 1 \leq \xi \leq 1 \tag{41}$$

Table 1 Boundary conditions

Boundary Conditions	S-S	C-S	C-C	C-F
r	0	0	0	1
p	0	0	1	−1
q	0	1	0	1

The displacement vectors of the element are noted as follows:

$$\begin{cases} \overline{\boldsymbol{U}}^{\boldsymbol{T}} = [U_1 \quad U_2 \ldots U_N] e^{j\omega t} \\ \overline{\boldsymbol{W_b}}^{\boldsymbol{T}} = [B_1 \quad B_2 \ldots B_N] e^{j\omega t} \\ \overline{\boldsymbol{W_s}}^{\boldsymbol{T}} = [S_1 \quad S_2 \ldots S_N] e^{j\omega t} \\ \overline{\boldsymbol{W_z}}^{\boldsymbol{T}} = [Z_1 \quad S_2 \ldots S_N] e^{j\omega t} \end{cases} \tag{42}$$

So, the equations of $u[x(\xi)]$ and $w_{b,s,z}[x(\xi)]$ became:

$$\begin{cases} u(\xi) = [N_u]^T \overline{\boldsymbol{U}} \\ w_b(\xi) = [N_w]^T \overline{\boldsymbol{W_b}} \\ w_s(\xi) = [N_w]^T \overline{\boldsymbol{W_s}} \\ w_z(\xi) = [N_w]^T \overline{\boldsymbol{W_z}} \end{cases} \tag{43}$$

Therefore

$$\begin{aligned} [\mathrm{N}_u]^T &= \left[\frac{dX_1(\xi)}{dt} \; \frac{dX_2(\xi)}{dt} \; \frac{dX_3(\xi)}{dt} \; \frac{dX_4(\xi)}{dt} \; \cdots \; \frac{dX_N(\xi)}{dt} \right] \\ [\mathrm{N}_w]^T &= [X_1(\xi) \; X_2(\xi) \; X_3(\xi) \; X_4(\xi) \; \ldots \; X_N(\xi)] \end{aligned} \tag{44}$$

The Gauss-Lobatto node calculation ξ_j, $j = 1, 2, \ldots, N$. Defines the following displacement vectors:

$$\begin{cases} \overline{\boldsymbol{u}}^{\boldsymbol{T}} = [u(\xi_1) \; u(\xi_2) \; \ldots \; u(\xi_N)] \\ \overline{\boldsymbol{w}}_{\boldsymbol{b}}{}^{\boldsymbol{T}} = [w_b(\xi_1) \; w_b(\xi_2) \; \ldots \; w_b(\xi_N)] \\ \overline{\boldsymbol{w}}_{\boldsymbol{s}}{}^{\boldsymbol{T}} = [w_s(\xi_1) \; w_s(\xi_2) \; \ldots \; w_s(\xi_N)] \\ \overline{\boldsymbol{w}}_{\boldsymbol{z}}{}^{\boldsymbol{T}} = [w_z(\xi_1) \; w_z(\xi_2) \; \ldots \; w_z(\xi_N)] \end{cases} \tag{45}$$

By replacing the Gauss-Lobatto nodes in Equation (45), we obtain the transfer matrices **G**, as follows:

$$\begin{cases} \overline{\boldsymbol{u}}^{\boldsymbol{T}} = \boldsymbol{G_u} \, \overline{\boldsymbol{U}} \\ \overline{\boldsymbol{w}}_{\boldsymbol{b}} = \boldsymbol{G_b} \, \overline{\boldsymbol{W}}_{\boldsymbol{b}} \\ \overline{\boldsymbol{w}}_{\boldsymbol{s}} = \boldsymbol{G_s} \, \overline{\boldsymbol{W}}_{\boldsymbol{s}} \\ \overline{\boldsymbol{w}}_{\boldsymbol{z}} = \boldsymbol{G_z} \, \overline{\boldsymbol{W}}_{\boldsymbol{z}} \end{cases} \tag{46}$$

Were

$$\begin{cases} \boldsymbol{G_u} = [[\mathrm{N}_u](\xi_1) & [\mathrm{N}_u](\xi_2) & \dots & [\mathrm{N}_u](\xi_N)]^{\boldsymbol{T}} \\ \boldsymbol{G_b} = [[\mathrm{N}_w](\xi_1) & [\mathrm{N}_w](\xi_2) & \dots & [\mathrm{N}_w](\xi_N)]^{\boldsymbol{T}} \\ \boldsymbol{G_s} = [[\mathrm{N}_w](\xi_1) & [\mathrm{N}_w](\xi_2) & \dots & [\mathrm{N}_w](\xi_N)]^{\boldsymbol{T}} \\ \boldsymbol{G_z} = [[\mathrm{N}_w](\xi_1) & [\mathrm{N}_w](\xi_2) & \dots & [\mathrm{N}_w](\xi_N)]^{\boldsymbol{T}} \end{cases} \tag{47}$$

All knot distribution shapes for differencing and squaring are $[-1, 1]$. Therefore, in order to apply them in practice, the following modifications must be made to the differentiation and quadrature matrices,

$$\overline{\boldsymbol{C}} = \frac{L}{2}C, \quad \overline{\boldsymbol{A}}^{(1)} = \frac{2}{\mathrm{L}}A^{(1)}, \quad \overline{\boldsymbol{A}}^{(2)} = \frac{4}{\mathrm{L}^2}A^{(2)} \tag{48}$$

Where L is the length of the beam.

Equations (24)–(48) can be used to substitute energy Equations (18), (20), (22) and Lagrange's equations to get the governing equations of motion.

$$\left[\begin{bmatrix} [K]_{11} & [K]_{12} & [K]_{13} & [K]_{14} \\ & [K]_{22} & [K]_{23} & [K]_{24} \\ & & [K]_{33} & [K]_{34} \\ sym & & & [K]_{44} \end{bmatrix} - \omega^2 \begin{bmatrix} [M]_{11} & [M]_{12} & [M]_{13} & [0] \\ & [M]_{22} & [M]_{23} & [M]_{24} \\ & & [M]_{33} & [M]_{34} \\ sym & & & [M]_{44} \end{bmatrix}\right]$$

$$\begin{Bmatrix} \boldsymbol{u} \\ \boldsymbol{w_b} \\ \boldsymbol{w_s} \\ \boldsymbol{w_z} \end{Bmatrix} = [0] \tag{49}$$

Component of the mass matrix

$$\begin{cases} [M]_{11} = \overline{\boldsymbol{C}}[J_1 G_u \, G_u] \\ [M]_{12} = -\overline{\boldsymbol{C}}[J_2 G_u \, \overline{\boldsymbol{A}}^{(\mathbf{1})} G_b] \\ [M]_{13} = \overline{\boldsymbol{C}}[J_3 G_u \, \overline{\boldsymbol{A}}^{(\mathbf{1})} G_s] \\ [M]_{22} = \overline{\boldsymbol{C}}[J_1 G_b G_b + J_5 \overline{\boldsymbol{A}}^{(\mathbf{1})} G_b \overline{\boldsymbol{A}}^{(\mathbf{1})} G_b] \\ [M]_{23} = \overline{\boldsymbol{C}}[J_1 G_b G_s - J_4 \overline{\boldsymbol{A}}^{(\mathbf{1})} G_b \overline{\boldsymbol{A}}^{(\mathbf{1})} G_s] \\ [M]_{24} = \overline{\boldsymbol{C}}[J_8 G_b G_z] \\ [M]_{33} = \overline{\boldsymbol{C}}[J_1 G_s G_s + J_6 \overline{\boldsymbol{A}}^{(\mathbf{1})} G_s \overline{\boldsymbol{A}}^{(\mathbf{1})} G_s] \\ [M]_{34} = \overline{\boldsymbol{C}}[J_8 G_s G_z] \\ [M]_{44} = \overline{\boldsymbol{C}}[J_7 G_z G_z] \end{cases} \tag{50}$$

The components of the strain matrix

$$
\begin{cases}
[K]_{11} = \overline{\boldsymbol{C}}[I_1\overline{\boldsymbol{A}}^{(\mathbf{1})}G_u\overline{\boldsymbol{A}}^{(\mathbf{1})}G_u] \\
[K]_{12} = -\overline{\boldsymbol{C}}[I_2\overline{\boldsymbol{A}}^{(\mathbf{1})}G_u\overline{\boldsymbol{A}}^{(\mathbf{2})}G_b] \\
[K]_{13} = \overline{\boldsymbol{C}}[I_3\overline{\boldsymbol{A}}^{(\mathbf{1})}G_u\overline{\boldsymbol{A}}^{(\mathbf{2})}G_s] \\
[K]_{14} = \overline{\boldsymbol{C}}[I_8\overline{\boldsymbol{A}}^{(\mathbf{1})}G_uG_z] \\
[K]_{22} = \overline{\boldsymbol{C}}\left[\left(I_5+\frac{1}{2}I_{14}\right)\overline{\boldsymbol{A}}^{(\mathbf{2})}G_b\overline{\boldsymbol{A}}^{(\mathbf{2})}G_b\right] - N_0\overline{\boldsymbol{C}}[\overline{\boldsymbol{A}}^{(\mathbf{1})}G_b\overline{\boldsymbol{A}}^{(\mathbf{1})}G_b] \\
[K]_{23} = \overline{\boldsymbol{C}}\left[\left(\frac{1}{4}I_{15}-I_4\right)\overline{\boldsymbol{A}}^{(\mathbf{2})}G_b\overline{\boldsymbol{A}}^{(\mathbf{2})}G_s\right] - N_0\overline{\boldsymbol{C}}[\overline{\boldsymbol{A}}^{(\mathbf{1})}G_b\overline{\boldsymbol{A}}^{(\mathbf{1})}G_s] \\
[K]_{24} = \overline{\boldsymbol{C}}\left[-I_9\overline{\boldsymbol{A}}^{(\mathbf{2})}G_bG_z+\frac{1}{4}I_{18}\overline{\boldsymbol{A}}^{(\mathbf{2})}G_b\overline{\boldsymbol{A}}^{(\mathbf{2})}G_z\right] \\
[K]_{33} = \overline{\boldsymbol{C}}\Bigg[\left(I_6+\frac{1}{8}I_{16}\right)\overline{\boldsymbol{A}}^{(\mathbf{2})}G_s\overline{\boldsymbol{A}}^{(\mathbf{2})}G_s \\
\qquad\qquad +\left(I_{11}+\frac{1}{8}I_{20}\right)\overline{\boldsymbol{A}}^{(\mathbf{1})}G_s\overline{\boldsymbol{A}}^{(\mathbf{1})}G_s\Bigg] - N_0\overline{\boldsymbol{C}}\left[\overline{\boldsymbol{A}}^{(\mathbf{1})}G_s\overline{\boldsymbol{A}}^{(\mathbf{1})}G_s\right] \\
[K]_{34} = \overline{\boldsymbol{C}}\Bigg[I_{10}\overline{\boldsymbol{A}}^{(\mathbf{2})}G_sG_z+\left(I_{12}-\frac{1}{8}I_{22}\right)\overline{\boldsymbol{A}}^{(\mathbf{1})}G_s\overline{\boldsymbol{A}}^{(\mathbf{1})}G_z \\
\qquad\qquad +\frac{1}{8}I_{17}\overline{\boldsymbol{A}}^{(\mathbf{2})}G_s\overline{\boldsymbol{A}}^{(\mathbf{2})}G_z\Bigg] \\
[K]_{44} = \overline{\boldsymbol{C}}\Bigg[J_7G_zG_z+\left(J_{13}+\frac{1}{8}J_{21}\right)\overline{\boldsymbol{A}}^{(\mathbf{1})}G_z\overline{\boldsymbol{A}}^{(\mathbf{1})}G_z \\
\qquad\qquad +\frac{1}{8}J_{19}\overline{\boldsymbol{A}}^{(\mathbf{2})}G_z\overline{\boldsymbol{A}}^{(\mathbf{2})}G_z\Bigg]
\end{cases}
\tag{51}
$$

3 Discussion of Results

A microbeam made of Aluminium/Silicon-carbide (Al/SiC) porous functionally graded material is studied in this section with MLSP based on (MCST). The material properties for the 2D-FG porous microbeam are assumed in the current analysis as follow. For the ceramic part the Young's modulus

$E_c = 427$ GPa, the mass density $\rho_c = 3100$ Kg/m^3, Poisson's ratio $\nu_c = 0.17$ and the MLSP $l_c = 22.5$ μm. For the metal part the Young's modulus $E_m = 70$ GPa, the mass density $\rho_c = 2702$ Kg/m^3, Poisson's ratio $\nu_c = 0.3$ and the MLSP $l_m = 15$ μm.

The following nondimensional parameters are introduced to simplify the results for the FG porous microbeam.

Dimensionless fundamental frequency (DFF) $(\overline{\omega})$

$$\overline{\omega} = \frac{\omega L^2}{h}\sqrt{\frac{\rho_m}{E_m}} \tag{52}$$

Dimensionless critical buckling load (DCBL)

$$\overline{N} = N_0 \frac{12L^2}{E_c b h^3} \tag{53}$$

In the convergence section, we have two cases for convergence. The first case represented by Tables 2–3, illustrates the convergence results of both dimensionless fundamental frequency and dimensionless critical buckling parameters for a perfect 2D-FG microbeam for different fraction volume indices in both directions k_x and k_z, and different boundary conditions (SS, CC, CF). The second case represented by Tables 4–5 illustrates the same thing for porous 2D-FG microbeam. From the convergence results in Tables 2–5, the dimensionless fundamental frequency parameters and the dimensionless critical buckling parameters converges quickly with *N* sampling points equal 7 to 10 demonstrating the efficacy of the resolution approach used and to ensure a good validation with the literature. In the following, we will choose a number of sampling N = 20. Because according to the convergence results the frequency parameters have already been converged.

Table 2 Convergence of DFF for the 2D-FG perfect microbeams with $(L/h = 5, h/l = 2, l_c = l_m)$

	DFF											
	SS				CC				CF			
	$k_x = 0$		$k_x = 2$		$k_x = 0$		$k_x = 2$		$k_x = 0$		$k_x = 2$	
N	$k_z = 0$	$k_z = 1$	$k_z = 0$	$k_z = 1$	$k_z = 0$	$k_z = 1$	$k_z = 0$	$k_z = 1$	$k_z = 0$	$k_z = 1$	$k_z = 0$	$k_z = 1$
5	9.4677	7.1235	6.1753	5.1450	18.9728	6.9854	5.8526	4.9328	3.6629	2.7577	1.9311	1.7581
6	9.4764	7.1303	6.1844	5.1518	19.0126	14.6040	13.8354	11.2777	3.6449	2.7442	1.9264	1.7520
7	9.4841	7.1356	6.1922	5.1573	19.8321	15.0279	13.6209	11.1841	3.6470	2.7457	1.9272	1.7528
8	9.4839	7.1354	6.1920	5.1572	20.0446	15.1925	13.8070	11.3274	3.6471	2.7458	1.9272	1.7529
9	9.4837	7.1353	6.1918	5.1570	20.4773	15.5243	14.1865	11.6195	3.6471	2.7458	1.9272	1.7529
10	9.4837	7.1353	6.1918	5.1570	20.4428	15.4977	14.1563	11.5962	3.6471	2.7458	1.9272	1.7529
20	9.4837	7.1353	6.1918	5.1570	20.4428	15.4977	14.1563	11.5962	3.6471	2.7458	1.9272	1.7529
30	9.4837	7.1353	6.1918	5.1570	20.4428	15.4977	14.1563	11.5962	3.6471	2.7458	1.9272	1.7529

Table 3 Convergence of DCBL for the 2D-FG perfect microbeams with ($L/h = 5$, $h/l = 2, l_c = l_m$)

	DCBL											
	SS				CC				CF			
	$k_x = 0$		$k_x = 2$		$k_x = 0$		$k_x = 2$		$k_x = 0$		$k_x = 2$	
N	$k_z = 0$	$k_z = 1$	$k_z = 0$	$k_z = 1$	$k_z = 0$	$k_z = 1$	$k_z = 0$	$k_z = 1$	$k_z = 0$	$k_z = 1$	$k_z = 0$	$k_z = 1$
5	19.7494	10.9941	8.3230	5.6687	66.2980	12.3510	8.3215	5.7955	5.6575	3.0077	1.5109	1.1943
6	21.3992	11.3913	8.3251	5.6684	70.0058	37.7366	33.6399	21.3966	5.5989	2.9763	1.5027	1.1854
7	21.3644	11.3711	8.3191	5.6621	71.5022	39.8331	30.0585	19.9139	5.6049	2.9795	1.5038	1.1864
8	21.3644	11.3711	8.3189	5.6621	74.5748	40.6761	30.8755	20.4216	5.6054	2.9797	1.5039	1.1865
9	21.3644	11.3711	8.3188	5.6620	74.4801	42.4066	32.5647	21.4701	5.6054	2.9797	1.5039	1.1864
10	21.3644	11.3711	8.3188	5.6620	74.3280	42.2676	32.4289	21.3857	5.6054	2.9797	1.5039	1.1864
20	21.3644	11.3711	8.3188	5.6620	74.3280	42.2676	32.4288	21.3857	5.6054	2.9797	1.5039	1.1864
30	21.3644	11.3711	8.3188	5.6620	74.3280	42.2676	32.4288	21.3857	5.6054	2.9797	1.5039	1.1864

Table 4 Convergence of DFF for the 2D-FG porous microbeams with ($\alpha_0 = 0.1, L/h = 5$, $h/l = 2, l_c = l_m$)

	DFF											
	SS				CC				CF			
	$k_x = 0$		$k_x = 2$		$k_x = 0$		$k_x = 2$		$k_x = 0$		$k_x = 2$	
N	$k_z = 0$	$k_z = 1$	$k_z = 0$	$k_z = 1$	$k_z = 0$	$k_z = 1$	$k_z = 0$	$k_z = 1$	$k_z = 0$	$k_z = 1$	$k_z = 0$	$k_z = 1$
5	9.1735	6.6774	5.7397	4.5723	8.6878	6.6416	5.4394	4.4253	3.5424	2.5785	1.7130	1.5026
6	9.1819	6.6839	5.7488	4.5788	18.3682	13.7737	12.9366	10.1519	3.5251	2.5658	1.7100	1.4982
7	9.1895	6.6886	5.7565	4.5839	19.1594	14.0885	12.7201	10.0054	3.5271	2.5673	1.7106	1.4989
8	9.1893	6.6885	5.7563	4.5838	19.3634	14.2432	12.8980	10.1381	3.5272	2.5674	1.7106	1.4989
9	9.1891	6.6883	5.7561	4.5837	19.7788	14.5536	13.2606	10.4082	3.5272	2.5674	1.7106	1.4989
10	9.1891	6.6883	5.7561	4.5837	19.7456	14.5287	13.2317	10.3867	3.5272	2.5674	1.7106	1.4989
20	9.1891	6.6883	5.7561	4.5837	19.7456	14.5287	13.2317	10.3867	3.5272	2.5674	1.7106	1.4989
30	9.1891	6.6883	5.7561	4.5837	19.7456	14.5287	13.2317	10.3867	3.5272	2.5674	1.7106	1.4989

Table 5 Convergence of DCBL for the 2D-FG porous microbeams with ($\alpha_0 = 0.1, L/h = 5, h/l = 2, l_c = l_m$)

	DCBL											
	SS				CC				CF			
	$k_x = 0$		$k_x = 2$		$k_x = 0$		$k_x = 2$		$k_x = 0$		$k_x = 2$	
N	$k_z = 0$	$k_z = 1$	$k_z = 0$	$k_z = 1$	$k_z = 0$	$k_z = 1$	$k_z = 0$	$k_z = 1$	$k_z = 0$	$k_z = 1$	$k_z = 0$	$k_z = 1$
5	16.7154	8.8517	6.4395	4.0023	18.1717	9.8853	6.4381	4.1677	4.7973	2.3685	1.0733	0.7838
6	18.1715	9.0011	6.4424	4.0030	55.9549	29.3196	26.8216	15.7731	4.7477	2.3438	1.0689	0.7787
7	18.1422	8.9847	6.4387	3.9990	59.0687	29.8650	23.4443	14.2340	4.7528	2.3463	1.0696	0.7793
8	18.1422	8.9847	6.4386	3.9989	60.3224	30.5182	24.0961	14.6094	4.7532	2.3465	1.0696	0.7794
9	18.1421	8.9847	6.4384	3.9988	62.8960	31.8466	25.4434	15.3848	4.7532	2.3465	1.0696	0.7794
10	18.1421	8.9847	6.4384	3.9988	62.6893	31.7392	25.3350	15.3223	4.7532	2.3465	1.0696	0.7794
20	18.1421	8.9847	6.4384	3.9988	62.6893	31.7392	25.3350	15.3223	4.7532	2.3465	1.0696	0.7794
30	18.1421	8.9847	6.4384	3.9988	62.6893	31.7392	25.3350	15.3223	4.7532	2.3465	1.0696	0.7794

In order to examine the current models, a comparative study of dimensionless fundamental frequency and dimensionless critical buckling is first carried out with the literature. For a 2D-FG porous microbeam in Tables 6–7 with $l_c = l_m$. The material properties for the 2D-FG porous microbeam are

Table 6 Comparative investigations for various aspect ratios and gradient indices based on the DFFs of C-C 2D-FG porous microbeams ($\alpha_0 = 0.1, l_m/h = 0.15, l_c = l_m$)

L/h	k_x	Method	$k_z = 0$	$k_z = 1$	$k_z = 5$	$k_z = 10$
12	0	Present ($\varepsilon_z \neq 0$)	23.2119	15.6230	12.9759	12.3695
		[59] (FEM)	23.7744	15.8815	13.0625	12.4194
		[60] (DQM)	23.4313	16.0784	13.4679	12.8762
	1	Present ($\varepsilon_z \neq 0$)	15.8261	13.3166	12.1570	11.8483
		[59] (FEM)	15.7363	13.3487	12.1727	11.8631
		[60] (DQM)	15.9708	13.7593	12.6711	12.1504
	5	Present ($\varepsilon_z \neq 0$)	12.3370	11.8131	11.5620	11.4759
		[59] (FEM)	12.4628	11.9103	11.6172	11.5206
		[60] (DQM)	12.8238	12.3764	12.1504	12.0730
18	0	Present ($\varepsilon_z \neq 0$)	24.0368	16.1882	13.2853	12.6650
		[59] (FEM)	24.2657	16.2084	13.3671	12.7092
		[60] (DQM)	24.0340	16.4872	13.8296	13.2224
	1	Present ($\varepsilon_z \neq 0$)	16.1570	13.6011	12.4379	12.1214
		[59] (FEM)	16.1678	13.6281	12.4439	12.1274
		[60] (DQM)	16.3903	14.1134	13.0049	12.4664
	5	Present ($\varepsilon_z \neq 0$)	12.6136	12.0763	11.8235	11.7343
		[59] (FEM)	12.7278	12.1625	11.8697	11.7709
		[60] (DQM)	13.1532	12.6933	12.4664	12.3870

Table 7 Comparative investigations for various aspect ratios and gradient indices based on the DCBLs of C-C 2D-FG porous microbeams ($L/h = 40, h/l_m = 5, l_c = l_m$)

α_0	k_x	Method	$k_z = 0$	$k_x = 0.1$	$k_x = 0.5$	$k_x = 2$	$k_x = 6$
0	0	Present ($\varepsilon_z \neq 0$)	43.5651	41.5934	36.8637	32.4295	30.3817
		[59] (FEM)	46.9072	44.6636	39.2169	33.9166	31.3078
		[61] (DQM)	48.8871	45.1740	40.7701	35.3948	32.6857
	2	Present ($\varepsilon_z \neq 0$)	32.3204	31.6331	30.0452	28.5777	27.7830
		[59] (FEM)	32.8990	32.6283	30.7448	29.1715	28.3059
		[61] (DQM)	36.1409	35.5350	34.0439	32.2045	31.1965
	6	Present ($\varepsilon_z \neq 0$)	29.3430	28.9955	28.2020	27.4686	27.0524
		[59] (FEM)	29.6824	29.3969	28.6935	27.9522	27.5283
		[61] (DQM)	33.9679	33.5835	32.6386	31.4597	30.8114
0.1	0	Present ($\varepsilon_z \neq 0$)	39.3220	37.3459	32.5840	28.1240	26.1475
		[59] (FEM)	43.4190	41.1079	35.5980	30.2177	27.6552
		[61] (DQM)	43.0365	41.3188	36.8804	31.4834	28.7908
	2	Present ($\varepsilon_z \neq 0$)	28.1184	27.4314	25.8416	24.3796	23.6016
		[59] (FEM)	29.2270	28.6101	27.0997	25.5398	24.6934
		[61] (DQM)	32.2281	31.6270	30.1478	28.3310	27.3355
	6	Present ($\varepsilon_z \neq 0$)	25.1569	24.8097	24.0170	23.2882	22.8783
		[59] (FEM)	26.0302	25.7533	25.0675	24.3385	23.9256
		[61] (DQM)	30.0860	29.7043	28.7663	27.5988	26.9563

assumed in the current validation analysis as follow. For the ceramic part the Young's modulus $E_c = 349.55$ GPa, the mass density $\rho_c = 3800$ Kg/m^3, Poisson's ratio $\nu_c = 0.24$, and the MLSP $l_c = 22.5$ μm. For the metal part the Young's modulus $E_m = 201.04$ GPa, the mass density $\rho_c = 8166$ Kg/m^3, Poisson's ratio $\nu_c = 0.3262$, and the MLSP $l_m = 15$ μm. The following nondimensional parameters are introduced to simplify the results for the first validation:

$$\overline{\omega} = \omega L^2 \sqrt{\frac{\rho_c A}{E_c I}}, \quad A = b \int_{-\frac{h}{2}}^{\frac{h}{2}} dz, \quad I = b \int_{-\frac{h}{2}}^{\frac{h}{2}} z^2 dz \tag{54}$$

For the validation of the accuracy of the results obtained in this work with other research works in the literature, Tables 6–7 present the results provided from the current DQGM method compared with the classical finite elements method used in the work [59] and with the differential quadrature method (DQM) used in the work [60] and [61].

As shown in Table 6, the DFFs of 2D-FG CC porous microbeams are computed for various aspect ratios, k_z and k_x. The numerical results are validated with those reported by [60] based on TBT via DQM and [59] based on TSNDBT via FEM. We can notice that the results are slightly close.

By addressing the buckling issue of an imperfect CC microbeam made of 2D-FG materials for various aspect ratios, k_z, k_x, and the microporosity volume fraction coefficients as presented in Table 7, validation experiments are still ongoing in this section.

The results presented in [61] based on the EBT formulation and that in [59] are used for comparison with the results calculated by the present theory via DQGM. It is found that the stiffness of the porous Euler-Bernoulli 2D-FG microbeam is significantly higher than that modelled based on the present theory. It is well known that in EBT, a beam behaves more rigidly than in TBT, RBT and HBT. The current tabulated results and those published in the open literature are pretty close, with only a little gap difference, suggesting that the resolution approach used in this investigation is valid.

Tables 8 to 11 represent the DFFs and DCBLs of 2D-FG microbeams for various boundary conditions, volume fraction indexes in two direction, porosity volume fraction coefficients, aspect ratios, and MLSPs. It can be observed that the results for every example obtained via the use of VMLSP are consistently higher than those obtained through the use of the constant MLSP. It is noticed that the VMLSP causes the microbeam's stiffness to increase. Additionally, for all cases, an increase in the volume fraction indexes, k_z or k_x, results in a decrease in the DFFs and DCBLs. It is to

Table 8 DFFs of 2D-FG perfect microbeams for various volume fraction index, aspect ratios and boundary conditions. With $h/l_m = 2$

$\alpha_0 = 0$		SS				CC				CF			
	k_z	k_x				k_x				k_x			
		0	0.5	1	2	0	0.5	1	2	0	0.5	1	2
$L/h = 5$													
$l_c = l_m$	0	9.4837	8.2524	7.3666	6.1918	20.4428	17.4664	15.9081	14.1563	3.6471	2.7957	2.3521	1.9272
	0.5	7.9698	7.0228	6.3557	5.4974	17.2490	14.9487	13.7595	12.4488	3.0694	2.4316	2.1080	1.8077
	1	7.1353	6.3677	5.8340	5.1570	15.4977	13.6147	12.6496	11.5962	2.7458	2.2397	1.9864	1.7529
	2	6.2811	5.7177	5.3282	4.8355	13.6779	12.2707	11.5511	10.7699	2.4174	2.0554	1.8733	1.7032
$l_c \neq l_m$	0	12.4084	10.0357	8.5782	6.8484	26.9470	21.5383	19.1264	16.5992	4.7544	3.2582	2.6137	2.0412
	0.5	9.8244	8.1503	7.1171	5.9042	21.3801	17.5062	15.7542	13.9279	3.7713	2.7243	2.2716	1.8772
	1	8.5882	7.2422	6.4185	5.4640	18.7983	13.0357	14.2049	12.7308	3.2927	2.4640	2.1098	1.8043
	2	7.3352	6.3410	5.7387	5.0468	16.1510	13.7537	12.6803	11.5772	2.8105	2.2117	1.9576	1.7378
$L/h= 10$													
$l_c = l_m$	0	9.8052	8.5491	7.6256	6.3923	22.2393	19.0190	17.3669	15.5212	3.6895	2.8236	2.3740	1.9441
	0.5	8.2373	7.2714	6.5771	5.6773	18.7267	16.2497	14.9971	13.6261	3.1053	2.4564	2.1283	1.8243
	1	7.3731	6.5917	6.0377	5.3290	16.7780	14.7750	13.7710	12.6820	2.7785	2.2634	2.0062	1.7696
	2	6.4944	5.9225	5.5192	5.0037	14.7883	13.3219	12.5867	11.7902	2.4475	2.0783	1.8929	1.7204
$l_c \neq l_m$	0	12.8044	10.3754	8.8618	7.0590	29.0916	23.2942	20.7529	18.1097	4.8049	3.2878	2.6360	2.0577
	0.5	10.1408	8.4277	7.3552	6.0905	23.0701	18.9320	17.0929	15.1897	3.8122	2.7502	2.2919	1.8934
	1	8.8570	7.4836	6.6316	5.6388	20.1866	16.8500	15.3736	13.8570	3.3288	2.4880	2.1293	1.8205
	2	7.5618	6.5517	5.9313	5.2137	17.2681	14.7980	13.7092	12.5956	2.8422	2.2342	1.9765	1.7541
$L/h = 20$													
$l_c = l_m$	0	9.8939	8.6314	7.6973	6.4473	22.8124	19.5157	17.8369	15.9658	3.7005	2.8308	2.3795	1.9484
	0.5	8.3112	7.3404	6.6384	5.7267	19.1969	16.6650	15.3949	14.0084	3.1145	2.4628	2.1335	1.8285
	1	7.4386	6.6538	6.0940	5.3763	17.1843	15.1450	14.1312	13.0345	2.7870	2.2695	2.0113	1.7739
	2	6.5533	5.9793	5.5721	5.0502	15.1414	13.6587	12.9211	12.1228	2.4552	2.0841	1.8980	1.7249
$l_c \neq l_m$	0	12.9116	10.4686	8.9393	7.1162	29.7467	23.8409	21.2660	18.5946	4.8178	3.2954	2.6416	2.0619
	0.5	10.2271	8.5041	7.4206	6.1414	23.5930	19.3793	17.5176	15.5961	3.8227	2.7568	2.2971	1.8975
	1	8.9301	7.5500	6.6901	5.6866	20.6127	17.2309	15.7430	14.2186	3.3380	2.4942	2.1343	1.8246
	2	7.6233	6.6095	5.9842	5.2594	17.6085	15.1236	14.0344	12.9228	2.8502	2.2399	1.9813	1.7583

Table 9 DCBLs of 2D-FG perfect microbeams for various volume fraction index, aspect ratios and boundary conditions. With $h/l_m = 2$

$\alpha_0 = 0$		SS				CC				CF			
	k_z	k_x				k_x				k_x			
		0	0.5	1	2	0	0.5	1	2	0	0.5	1	2
$L/h = 5$													
$l_c = l_m$	0	21.5394	15.7731	12.3123	8.5085	74.3460	52.3401	42.3229	32.4698	5.6200	3.2651	2.2891	1.5127
	0.5	15.0619	11.3846	9.1618	6.7123	51.8550	37.8416	31.4056	25.0554	3.9329	2.4268	1.7981	1.2967
	1	12.3191	9.5187	7.8206	5.9462	42.2676	31.6213	26.7136	21.8666	3.2207	2.0715	1.5897	1.2049
	2	9.8255	7.8190	6.5974	5.2454	33.4320	25.8719	22.3745	18.9189	2.5765	1.7492	1.4004	1.1211
$l_c \neq l_m$	0	36.8582	23.2878	16.6715	10.4021	130.4227	80.0779	61.4818	44.8110	9.5422	4.4299	2.8235	1.6955
	0.5	22.6369	15.2112	11.4272	7.7262	79.6303	51.8805	41.1703	31.3704	5.8713	3.0304	2.0822	1.3970
	1	17.4753	12.1535	9.3937	6.6599	61.7298	41.5238	33.6190	26.3375	4.5272	2.4855	1.7867	1.2754
	2	13.0330	9.4770	7.5966	5.7063	46.1507	32.3916	26.9307	21.8675	3.3746	2.0063	1.5241	1.1662
L/h= 10													
$l_c = l_m$	0	22.4798	16.5314	12.8761	8.8374	86.1575	60.7634	49.3956	38.2265	5.6828	3.2910	2.3039	1.5208
	0.5	15.7318	11.9358	9.5870	6.9832	60.2474	44.0242	36.7129	29.5117	3.9778	2.4472	1.8108	1.3049
	1	12.8827	9.9893	8.1927	6.1967	49.2764	36.9113	31.3193	25.8049	3.2585	2.0899	1.6020	1.2134
	2	10.3062	8.2258	6.9283	5.4825	39.3021	30.4319	26.4039	22.4268	2.6089	1.7665	1.4128	1.1303
$l_c \neq l_m$	0	38.1689	24.2205	17.2984	10.7297	147.4327	91.0802	70.4593	51.9840	9.6290	4.4574	2.8378	1.7027
	0.5	23.4853	15.8517	11.8866	7.9964	90.5474	59.3571	47.4411	36.5415	5.9276	3.0515	2.0945	1.4044
	1	18.1088	12.6582	9.7729	6.9014	69.9010	47.4318	38.7010	30.6480	4.5692	2.5033	1.7980	1.2830
	2	13.4983	9.8726	7.9110	5.9260	52.1320	37.0268	31.0424	25.4716	3.4054	2.0217	1.5349	1.1742
$L/h = 20$													
$l_c = l_m$	0	22.7313	16.7354	13.0273	8.9246	89.9194	63.4521	51.6733	40.1082	5.6988	3.2975	2.3077	1.5229
	0.5	15.9110	12.0842	9.7011	7.0552	62.9272	46.0016	38.4241	30.9674	3.9892	2.4523	1.8141	1.3069
	1	13.0338	10.1161	8.2928	6.2635	51.5307	38.6149	32.8134	27.0967	3.2681	2.0946	1.6051	1.2155
	2	10.4358	8.3359	7.0176	5.5460	41.2247	31.9242	27.7292	23.5887	2.6172	1.7709	1.4159	1.1326
$l_c \neq l_m$	0	38.5159	24.4690	17.4647	10.8157	152.6755	94.5032	73.2880	54.2921	9.6510	4.4643	2.8415	1.7046
	0.5	23.7105	16.0228	12.0090	8.0677	93.9412	61.7013	49.4302	38.2119	5.9419	3.0568	2.0976	1.4063
	1	18.2768	12.7930	9.8739	6.9653	72.4351	49.2854	40.3148	32.0411	4.5799	2.5078	1.8009	1.2849
	2	13.6218	9.9785	7.9949	5.9843	53.9930	38.4909	32.3571	26.6424	3.4133	2.0256	1.5376	1.1762

Table 10 DFFs of 2D-FG porous microbeams for various volume fraction index, aspect ratios and boundary conditions. With $h/l_m = 2$

$\alpha_0 = 0$		SS				CC				CF			
	k_z	k_x				k_x				k_x			
		0	0.5	1	2	0	0.5	1	2	0	0.5	1	2
$L/h = 5$													
$l_c = l_m$	0	8.9109	7.6199	6.6555	5.3047	19.1067	15.9847	14.2864	12.2944	3.4192	2.5056	1.9994	1.4691
	0.5	7.2257	6.1920	5.4324	4.3966	15.6050	13.0912	11.7353	10.1713	2.7725	2.0623	1.6755	1.2819
	1	6.2098	5.3540	4.7335	3.9038	13.5052	11.4014	10.2791	8.9993	2.3772	1.8014	1.4938	1.1863
	2	5.0869	4.4577	4.0092	3.4200	11.1566	9.5758	8.7430	7.8015	1.9424	1.5305	1.3147	1.0988
$l_c \neq l_m$	0	11.5404	9.1214	7.6202	5.7775	25.0084	19.5199	17.0596	14.4255	4.4118	2.8747	2.1923	1.5413
	0.5	8.8371	7.0925	5.9954	4.6532	19.2285	15.2103	13.3666	11.3894	3.3808	2.2806	1.7832	1.3145
	1	7.4780	6.0494	5.1577	4.0845	16.4128	13.0702	11.5457	9.9243	2.8535	1.9660	1.5705	1.2044
	2	6.0303	4.9581	4.3020	3.5304	13.3727	10.8116	9.6604	8.4480	2.2946	1.6437	1.3621	1.1039
L/h= 10													
$l_c = l_m$	0	9.2157	7.8984	6.8906	5.4695	20.8459	17.4506	15.6407	13.5318	3.4606	2.5309	2.0176	1.4813
	0.5	7.4639	6.4087	5.6172	4.5307	16.9361	14.2163	12.7794	11.1343	2.8059	2.0834	1.6912	1.2929
	1	6.4091	5.5363	4.8919	4.0240	14.5675	12.3168	11.1404	9.8103	2.4065	1.8209	1.5086	1.1970
	2	5.2499	4.6095	4.1456	3.5308	11.9537	10.2987	9.4451	8.4899	1.9682	1.5487	1.3291	1.1095
$l_c \neq l_m$	0	11.9023	9.4290	7.8689	5.9464	27.0010	21.1289	18.5345	15.7759	4.4603	2.9013	2.2109	1.5533
	0.5	9.1120	7.3280	6.1891	4.7896	20.7083	16.4189	14.4790	12.4133	3.4185	2.3026	1.7991	1.3254
	1	7.7005	6.2424	5.3201	4.2045	17.5430	14.0189	12.4327	10.7585	2.8860	1.9860	1.5853	1.2148
	2	6.2059	5.1135	4.4378	3.6382	14.1754	11.5249	10.3505	9.1262	2.3228	1.6620	1.3761	1.1141
$L/h = 20$													
$l_c = l_m$	0	9.2998	7.9758	6.9556	5.5145	21.4025	17.9202	16.0777	13.9366	3.4714	2.5375	2.0223	1.4843
	0.5	7.5294	6.4687	5.6681	4.5673	17.3580	14.5732	13.1130	11.4460	2.8145	2.0889	1.6953	1.2957
	1	6.4638	5.5867	4.9355	4.0568	14.9015	12.6053	11.4140	10.0714	2.4141	1.8259	1.5124	1.1998
	2	5.2947	4.6516	4.1833	3.5612	12.2032	10.5265	9.6685	8.7122	1.9749	1.5533	1.3328	1.1123
$l_c \neq l_m$	0	12.0010	9.5137	7.9370	5.9921	27.6189	21.6351	19.0041	16.2140	4.4727	2.9081	2.2156	1.5564
	0.5	9.1871	7.3930	6.2422	4.8266	21.1686	16.7984	14.8319	12.7435	3.4282	2.3082	1.8032	1.3281
	1	7.7610	6.2954	5.3646	4.2370	17.8897	14.3137	12.7114	11.0252	2.8944	1.9911	1.5891	1.2175
	2	6.2534	5.1561	4.4749	3.6675	14.4181	11.7448	10.5663	9.3425	2.3300	1.6667	1.3797	1.1168

Table 11 DCBLs of 2D-FG porous microbeams for various volume fraction index, aspect ratios and boundary conditions. With $h/l_m = 2$

$\alpha_0 = 0$		SS				CC				CF			
	k_z	k_x				k_x				k_x			
		0	0.5	1	2	0	0.5	1	2	0	0.5	1	2
$L/h = 5$													
$l_c = l_m$	0	15.3445	10.7374	7.9675	4.9089	52.5045	35.0996	27.1436	19.3039	4.0137	2.1245	1.3365	0.7078
	0.5	10.1195	7.1884	5.4137	3.4492	34.6230	23.5484	18.4463	13.4042	2.6469	1.4417	0.9359	0.5317
	1	7.9654	5.7195	4.3568	2.8460	27.0888	18.6552	14.7536	10.8935	2.0878	1.1620	0.7719	0.4596
	2	6.0371	4.4017	3.4083	2.3045	20.1571	14.1423	11.3442	8.5747	1.5927	0.9141	0.6265	0.3956
$l_c \neq l_m$	0	25.7511	15.3797	10.4444	5.8270	90.6046	52.5805	38.8466	26.6532	6.6784	2.7943	1.6055	0.7785
	0.5	14.8785	9.3190	6.5421	3.8521	52.1347	31.5830	23.7996	16.7321	3.8635	1.7465	1.0545	0.5582
	1	11.0950	7.1178	5.0916	3.0992	39.0076	24.0988	18.3651	13.1188	2.8784	1.3572	0.8453	0.4730
	2	7.9214	5.2400	3.8436	2.4452	27.7745	17.5982	13.6177	9.9488	2.0575	1.0255	0.6655	0.3991
$L/h= 10$													
$l_c = l_m$	0	16.0550	11.2902	8.3523	5.0952	61.3782	41.0780	31.9554	22.9765	4.0613	2.1410	1.3443	0.7106
	0.5	10.5876	7.5551	5.6736	3.5817	40.4779	27.5398	21.6921	15.9244	2.6782	1.4531	0.9416	0.5340
	1	8.3512	6.0235	4.5751	2.9616	31.8616	21.9440	17.4463	13.0050	2.1137	1.1718	0.7770	0.4619
	2	6.3709	4.6653	3.6005	2.4112	24.1485	16.9279	13.6380	10.3855	1.6154	0.9231	0.6313	0.3981
$l_c \neq l_m$	0	26.7137	16.0360	10.8567	6.0068	103.0046	60.1958	44.8427	31.2079	6.7423	2.8115	1.6130	0.7810
	0.5	15.4541	9.7301	6.8124	3.9798	59.5141	36.2861	27.5591	19.6322	3.9018	1.7580	1.0599	0.5603
	1	11.5137	7.4310	5.3045	3.2059	44.3800	27.6671	21.2657	15.3956	2.9062	1.3664	0.8499	0.4750
	2	8.2301	5.4844	4.0167	2.5386	31.6858	20.3400	15.8920	11.7680	2.0781	1.0331	0.6696	0.4011
$L/h = 20$													
$l_c = l_m$	0	16.2452	11.4393	8.4557	5.1444	64.2199	42.9943	33.5127	24.1871	4.0734	2.1452	1.3463	0.7113
	0.5	10.7129	7.6539	5.7433	3.6168	42.3504	28.8160	22.7392	16.7515	2.6862	1.4559	0.9430	0.5346
	1	8.4549	6.1057	4.6339	2.9923	33.4050	23.0067	18.3239	13.7041	2.1203	1.1742	0.7782	0.4625
	2	6.4615	4.7373	3.6527	2.4398	25.4835	17.8569	14.4083	11.0011	1.6212	0.9253	0.6326	0.3987
$l_c \neq l_m$	0	26.9691	16.2114	10.9662	6.0539	106.8548	62.5821	46.7469	32.6897	6.7585	2.8159	1.6149	0.7817
	0.5	15.6070	9.8402	6.8844	4.0133	61.8163	37.7642	28.7551	20.5752	3.9115	1.7609	1.0613	0.5609
	1	11.6249	7.5148	5.3613	3.2339	46.0547	28.7910	22.1913	16.1381	2.9133	1.3687	0.8510	0.4755
	2	8.3123	5.5503	4.0631	2.5634	32.9202	21.2187	16.6312	12.3721	2.0833	1.0350	0.6707	0.4016

highlight that when the gradient index increases, the mass decreases at a slower rate than the stiffness. Additionally, in all circumstances, the DFFs and DCBLs are more significantly affected by the k_z. Moreover, when the porosity volume fraction coefficient rises, this effect becomes more obvious. The DFFs and DCBLs rise as the aspect ratio increases, as predicted. These findings might act as a baseline for further research.

Figure 2 depicts DFF variation for porous 2D-FG microbeams with respect to various aspect ratios, thickness to MLSPs, and boundary conditions. It is important to note that the significant size impact reduces when the aspect ratio drops. The small size impact is declining, notably for Clamped-Clamped boundary conditions, as the shear deformation effect increases. It is noteworthy that it is evident that the maximum difference between the DFFs was obtained by using L/h $= 3$ and L/h $= 5$. After setting the aspect ratio to 5, the slope of the curve is decreasing. We notice that the curves' maximum slope is attained by utilizing VMLSP and applying the Clamped-Clamped boundary conditions method. For all circumstances, the minimal slope is obtained using Clamped-Free boundary conditions. For all examples, the influence of aspect ratio variation on DFFs is more evident for microbeams with VMLSP.

It should be noted that the difference between the DFFs produced by setting the MLSPs to 1 and 2 is minimal for SS 2D-FG porous microbeams. It is, meanwhile, maximal for CF 2D-FG porous microbeams. For Clamped-Free microbeams, the impact of aspect ratio change is virtually non-existent for any thickness value to MLSP. The aspect ratio's impact on the DFFs of porous 2D-FG microbeams reduces as thickness to MLSP increases. Figure 3 illustrates how the DCBLs of 2D-FG porous microbeams vary with different aspect ratios, BCs, and thickness to MLSPs. The influence of these parameters on DCBLs are also explored. Moreover, it is observed that the impacts of the factors mentioned above are nearly identical to those discovered through analysis of free vibration behaviour. Also, because VMLSP increases the stiffness of the porous 2D-FG microbeams, the DFFs and DCBLs acquired using VMLSP are always more significant than those obtained using constant MLSP in all cases.

Figures 4–5 illustrate DFFs and DCBLs Variation for porous 2D-FG microbeams with respect to power indexes k_x, k_z, boundary conditions (SS, CC), equal MLSP and VMLSP. According to results in Figures 4–5, we notice that the increase of porosity volume fraction led to decreasing of both DFFs and DCBLs. The decreased gap defers from one FG mixture to another. The results of the curves according to volume fraction k_x are almost close to those

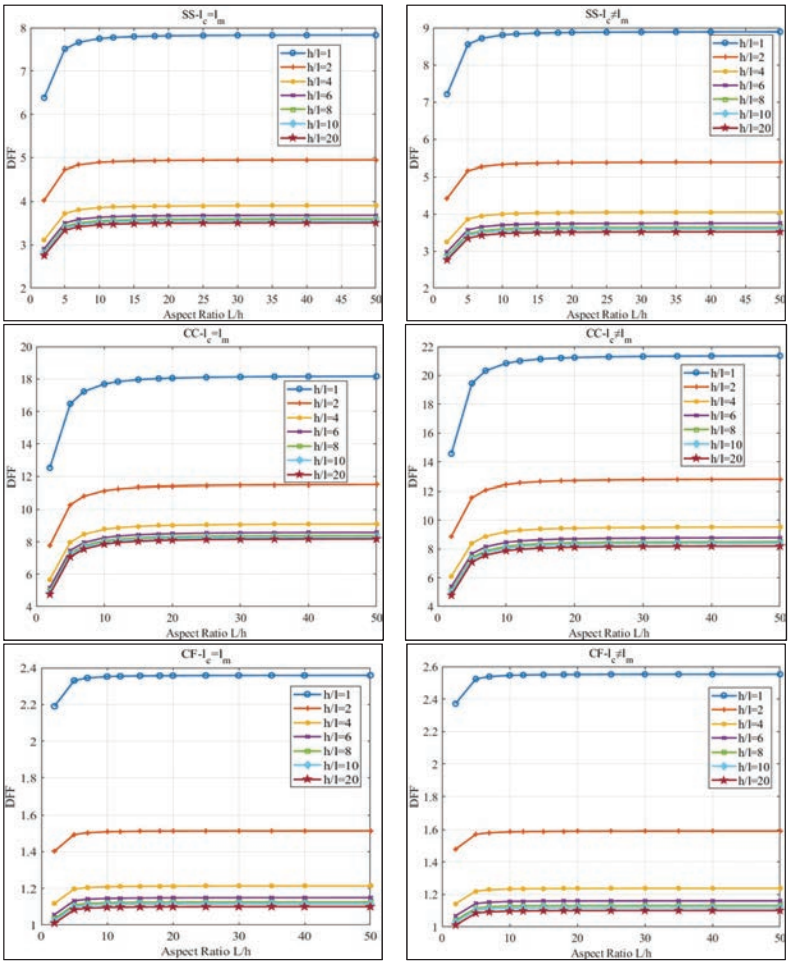

Figure 2 DFFs Variation for porous 2D-FG microbeams with respect to various aspect ratios, thickness to MLSPs, and boundary conditions, with ($k_z = 1$, $k_x = 1$, $\alpha = 0.2$).

according to volume fraction k_z. The gap in the results of DFFs and DCBLs between different porosity volume fraction, is less important in the VMLSP case compared to the equal MLSP case.

Figures 6–7 illustrate DFFs Variation for porous 2D-FG microbeams with respect to various FG volume fraction indexes k_x, k_z, thickness to MLSPs, and boundary conditions. It can be observed that the influence of k_x and k_z variation is considerable for the cases with VMLSP. Furthermore, when the thickness to MLSP (else referred to as determined using l_m) increases, the

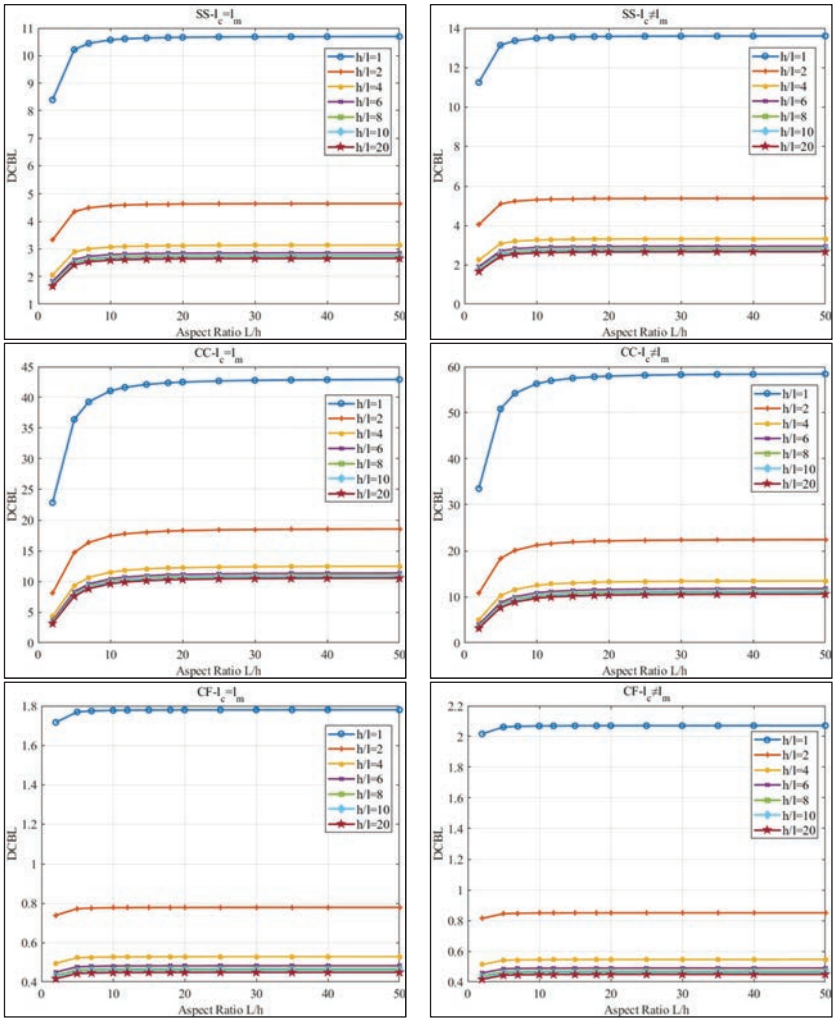

Figure 3 DCBLs Variation for porous 2D-FG microbeams with respect to various aspect ratios, thickness to MLSPs, and boundary conditions, with ($k_z = 1$, $k_x = 1$, $\alpha = 0.2$).

DFFs decrease in all circumstances. The small size influence clearly enhances the rigidity of the structure, and this influence is stronger with VMLSP.

The stiffness of the structure is seen to rise not only with the influence of the tiny size but also with the change of thickness to MLSP. It is noticed that the stiffness of the structure increases not only with the influence of the small size but also with the change of thickness to MLSP. It should be noted

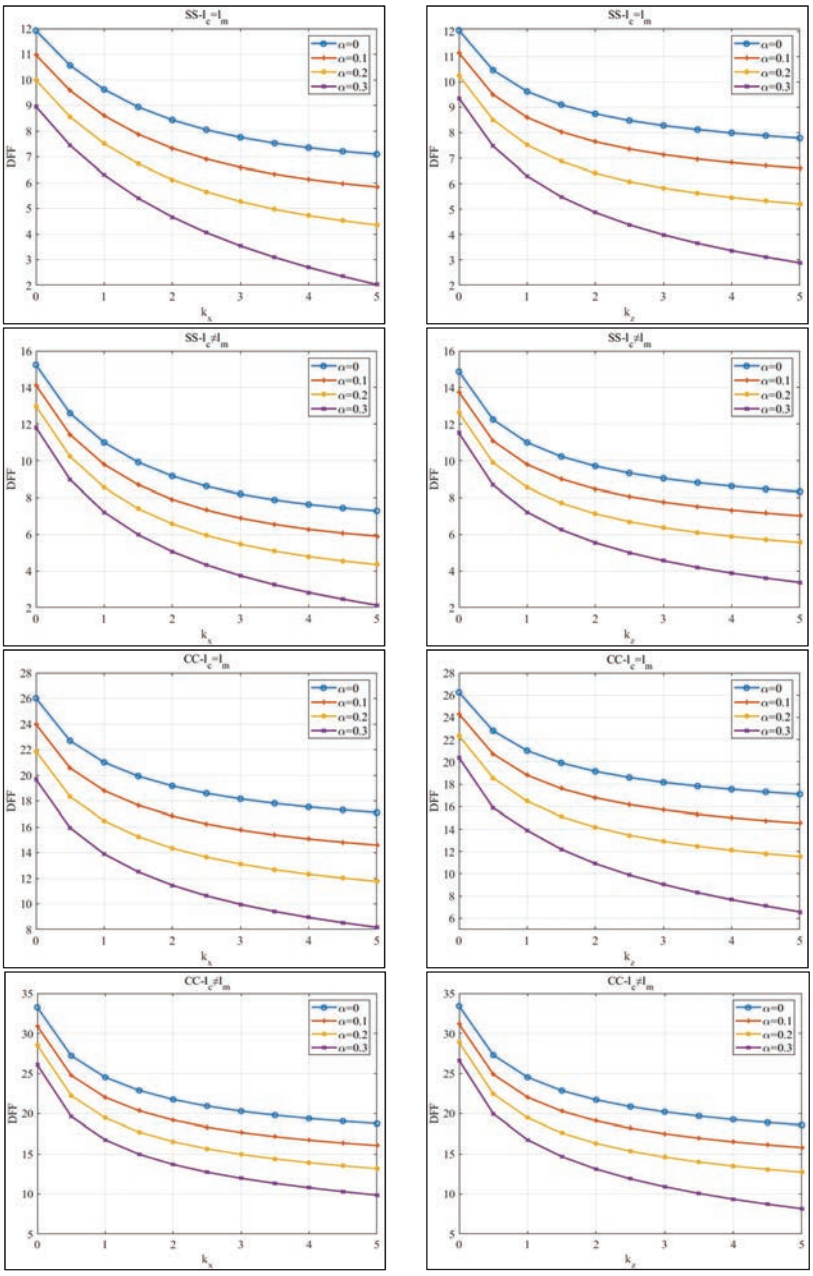

Figure 4 DFFs Variation for porous 2D-FG microbeams with respect to k_z and k_x, with $L/h = 5$, $h/l = 2$.

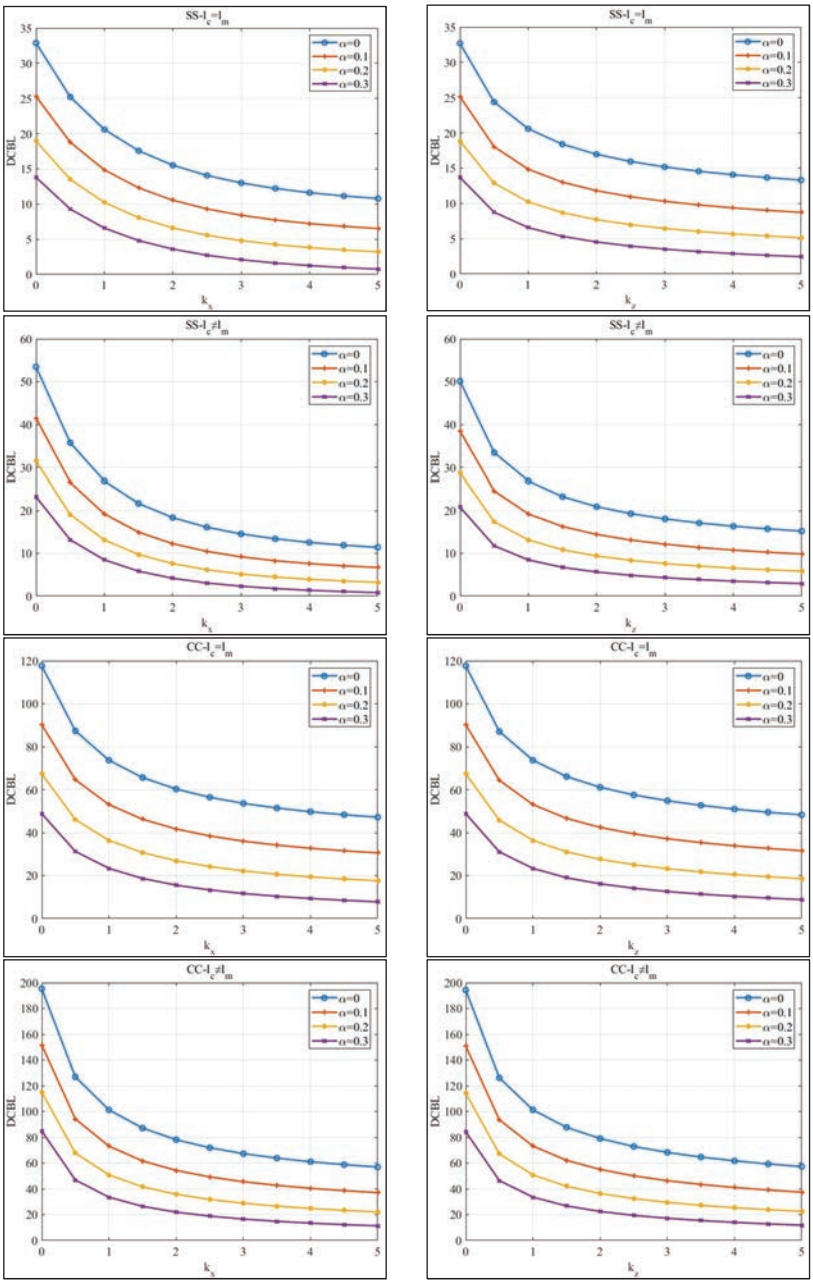

Figure 5 DCBLs Variation for porous 2D-FG microbeams with respect to k_z and k_x, with $L/h = 5$, $h/l = 2$.

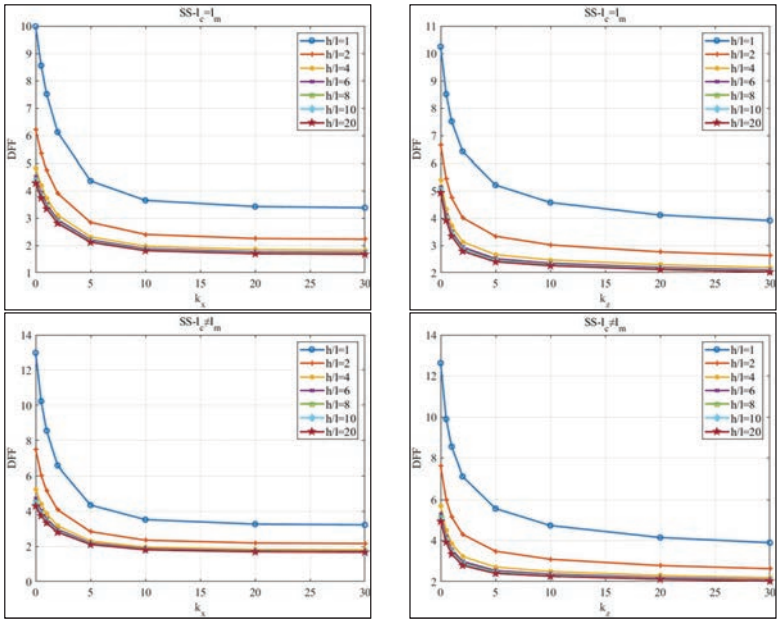

Figure 6 DFFs Variation for SS porous 2D-FG microbeams with respect to volume fraction indexes, thickness to MLSPs, with ($\mathrm{L/h} = 1$, $\alpha = 0.2$).

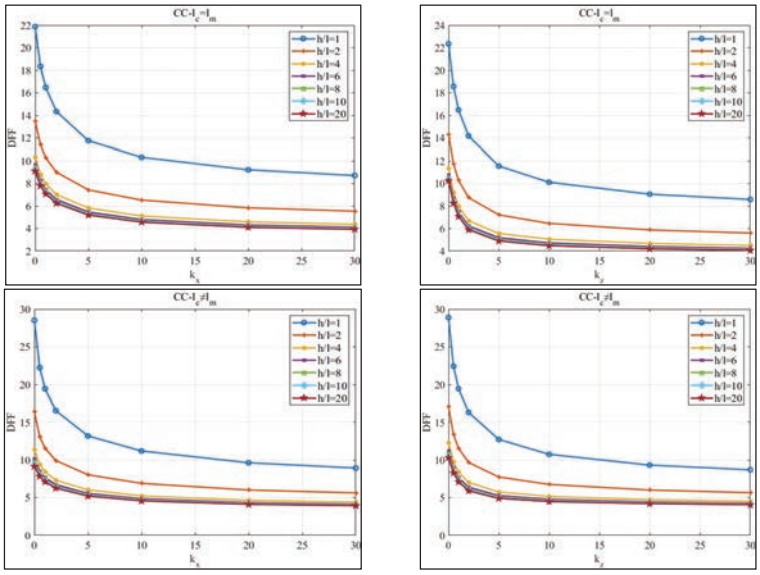

Figure 7 DFFs Variation for CC porous 2D-FG microbeams with respect to volume fraction indexes, thickness to MLSPs, with ($\mathrm{L/h} = 1$, $\alpha = 0.2$).

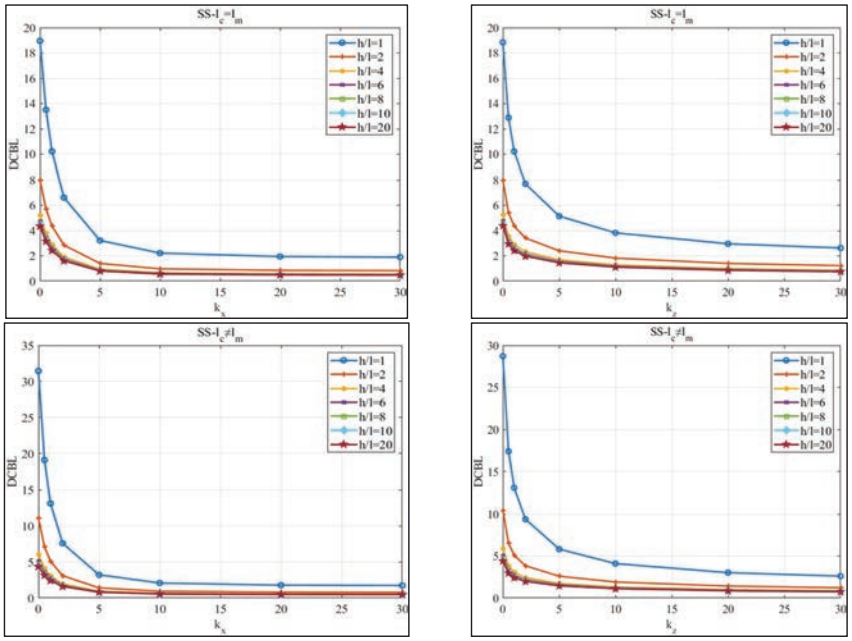

Figure 8 DCBLs Variation for SS porous 2D-FG microbeams with respect to volume fraction indexes, thickness to MLSPs, with ($\mathrm{L/h} = 1$, $\alpha = 0.2$).

that the influence of FG volume fraction indexes on DFFs decreases as the thickness of MLSP increases. One of the most essential things to note is that as the thickness of the MLSP increases, the impacts of the FG volume fraction indexes decrease.

Figures 8–9 illustrate DCBLs Variation for porous 2D-FG microbeams with respect to various FG volume fraction indexes k_x, k_z, thickness to MLSPs, and boundary conditions.

Figures 8–9 illustrate DCBLs Variation for porous 2D-FG microbeams with respect to various FG volume fraction indexes k_x, k_z, thickness to MLSPs, and boundary conditions. The effect of varying k_x and k_z on the DBCLs of a microbeam with VMLSP is clearly more noticeable than the effect of having constant MLSP. The microbeam is stiffer with VMLSP than with the constant MLSP. It is clear that the small size effect is important for microbeams with VMLSP. This effect, however, decreases as the gradient index increases in all circumstances. The smaller size effect is shown to diminish when the effective modulus of elasticity decreases. As previously stated, the greatest DCBLs are always attained by using VMLSP.

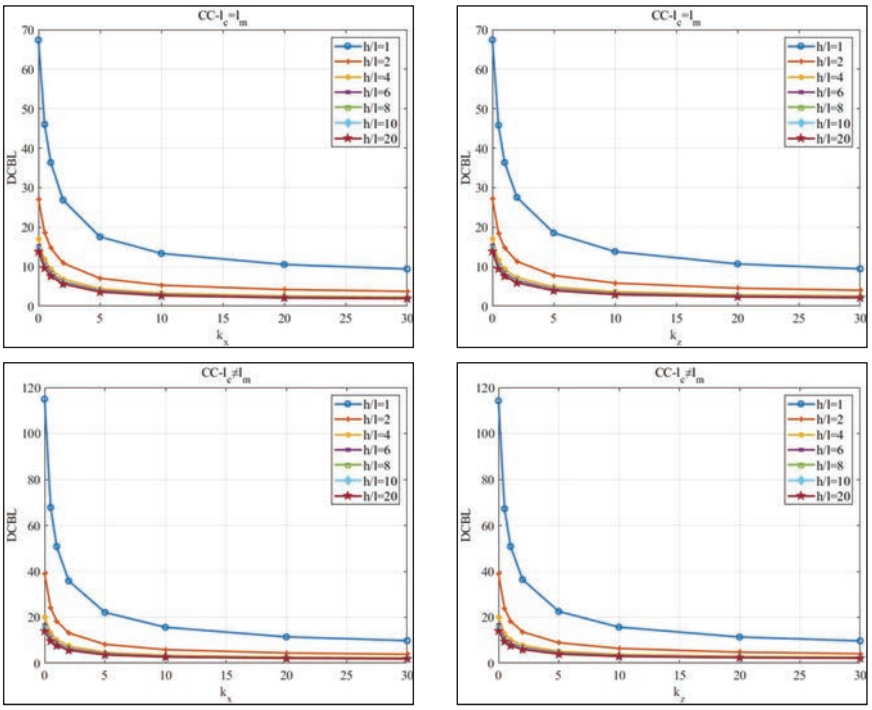

Figure 9 DCBLs Variation for CC porous 2D-FG microbeams with respect to volume fraction indexes, thickness to MLSPs, with ($\mathrm{L/h} = 1$, $\alpha = 0.2$).

4 Conclusion

The analysis of free vibration and buckling behaviours of porous 2D-FG microbeams are explored in this paper using the Quasi-3D beam deformation theory based on the modified couple stress theory and a Differential Quadrature Galerkin Method (DQGM) systematically, as a combination of the Differential Quadrature Method (DQM) and the semi analytical Galerkin method, which has used to reduced computational cost for problems in dynamics. The use of these method is new in the context of porous 2D-FG microbeams. The governing equations are obtained using the Lagrange's principle. The mass, gyroscopic and stiffness matrices are simply calculated using the weighting coefficient matrices given by the differential quadrature (DQ) and Gauss-Lobatto quadrature rules. The matrices are expressed in a similar form to that of the Differential Quadrature Method by introducing an interpolation basis on the element boundary of the Galerkin method. The sampling points are determined by the Gauss-Lobatto node method.

The impacts of the thickness to material length scale parameter (MLSP) on the nondimensional natural frequencies and nondimensional critical buckling loads of 2D-FG porous microbeams are investigated, along with the effects of the boundary condition, aspect ratio, and gradient index. To establish the accuracy of the procedure described, the results are well validated with literature methods, and the difference between the methods is small, which explains the efficiency of the methods. The convergence is obtained for a low sampling point compared to others methods in literatures. Several cases were handled, allowing us to evaluate the effects of various geometrical parameters of the porous 2D-FG microbeam.

This work allowed us to draw the following conclusions:

- The matrices of the DQGM are somewhat similar to those of the DQHFEM and DQFEM. The convergence of the results can be controlled by increasing the number of sampling points. The convergence can be obtained quickly with small sampling points, which mean small matrix size, and fast computation.
- The difference in results between the DQGM and literature methods is very small. The DQGM has the benefits of a simple mathematical concept, quick convergence speed, excellent computational accuracy, minimal computing amount, and lower memory requirements, among other things. According to the findings of this study.
- The rigidity of the microbeam increases as a result of VMLSP. As a result, DFFs and DCBLs calculated using the VMLSP are always higher than those calculated using the constant MLSP. The use of VMLSP, as well as the small size effect, enhances the rigidity of the microbeam. It was observed that raising the porosity volume fraction index causes a drop in stiffness, which causes a decrease in DFFs and DCBLs. For DFFs and DCBLs, the small size impact reduces as the aspect ratio drops. The increase in thickness to MLSPs ratio led to decrease both DFFs and DCBLs.

Disclosure Statement

No potential conflict of interest was reported by the author(s).

Data Availability Statement

The authors declare that the data are available within the article.

References

[1] T.-K. Nguyen, T. P. Vo, and H.-T. Thai, "Static and free vibration of axially loaded functionally graded beams based on the first-order shear deformation theory," *Composites Part B: Engineering*, vol. 55, pp. 147–157, 2013/12/01/ 2013, doi: https://doi.org/10.1016/j.compositesb.2013.06.011.

[2] S.-R. Li and R. C. Batra, "Relations between buckling loads of functionally graded Timoshenko and homogeneous Euler–Bernoulli beams," *Composite Structures*, vol. 95, pp. 5–9, 2013/01/01/ 2013, doi: https://doi.org/10.1016/j.compstruct.2012.07.027.

[3] T.-K. Nguyen and B.-D. Nguyen, "A new higher-order shear deformation theory for static, buckling and free vibration analysis of functionally graded sandwich beams," *Journal of Sandwich Structures & Materials*, vol. 17, no. 6, pp. 613–631, 2015, doi: 10.1177/1099636215589237.

[4] P. Van Vinh, "Deflections, stresses and free vibration analysis of bi-functionally graded sandwich plates resting on Pasternak's elastic foundations via a hybrid quasi-3D theory," *Mechanics Based Design of Structures and Machines*, pp. 1–32, 2021, doi: 10.1080/15397734.2021.1894948.

[5] B. Adhikari and B. N. Singh, "Dynamic response of functionally graded plates resting on two-parameter-based elastic foundation model using a quasi-3D theory," *Mechanics Based Design of Structures and Machines*, vol. 47, no. 4, pp. 399–429, 2019/07/04 2019, doi: 10.1080/15397734.2018.1555965.

[6] M. Nemat-Alla, "Reduction of thermal stresses by developing two-dimensional functionally graded materials," *International Journal of Solids and Structures*, vol. 40, no. 26, pp. 7339–7356, 2003/12/01/ 2003, doi: https://doi.org/10.1016/j.ijsolstr.2003.08.017.

[7] A. J. Goupee and S. S. Vel, "Optimization of natural frequencies of bidirectional functionally graded beams," *Structural and Multidisciplinary Optimization*, vol. 32, no. 6, pp. 473–484, 2006/12/01 2006, doi: 10.1007/s00158-006-0022-1.

[8] C. F. Lü, W. Q. Chen, R. Q. Xu, and C. W. Lim, "Semi-analytical elasticity solutions for bi-directional functionally graded beams," *International Journal of Solids and Structures*, vol. 45, no. 1, pp. 258–275, 2008/01/01/ 2008, doi: https://doi.org/10.1016/j.ijsolstr.2007.07.018.

[9] A. Karamanlı, "Bending behaviour of two directional functionally graded sandwich beams by using a quasi-3d shear deformation theory,"

Composite Structures, vol. 174, pp. 70–86, 2017/08/15/ 2017, doi: https://doi.org/10.1016/j.compstruct.2017.04.046.

[10] D. K. Nguyen, Q. H. Nguyen, T. T. Tran, and V. T. Bui, "Vibration of bi-dimensional functionally graded Timoshenko beams excited by a moving load," *Acta Mechanica*, vol. 228, no. 1, pp. 141–155, 2017/01/01 2017, doi: 10.1007/s00707-016-1705-3.

[11] A. Selmi, "Free vibration of bi-dimensional functionally graded simply supported beams," (in En), *Advances in concrete construction*, vol. 12, no. 3, pp. 195–205, 09/25 2021, doi: 10.12989/ACC.2021.12.3.195.

[12] S. N. Balireddy and J. Pitchaimani, "Stability and dynamic behaviour of bi-directional functionally graded beam subjected to variable axial load," *Materials Today Communications*, vol. 32, p. 104043, 2022/08/01/ 2022, doi: https://doi.org/10.1016/j.mtcomm.2022.104043.

[13] I. Bensaid, "A refined nonlocal hyperbolic shear deformation beam model for bending and dynamic analysis of nanoscale beams," (in En), *Advances in nano research*, vol. 5, no. 2, pp. 113–126, 06/25 2017, doi: 10.12989/ANR.2017.5.2.113.

[14] I. Bensaid and A. Guenanou, "Bending and stability analysis of size-dependent compositionally graded Timoshenko nanobeams with porosities," (in En), *Advances in materials Research*, vol. 6, no. 1, pp. 45–63, 03/25 2017, doi: 10.12989/AMR.2017.6.1.045.

[15] ª. D. Akbaº, "Forced vibration analysis of cracked functionally graded microbeams," *Advances in Nano Research*, vol. 6, no. 1, p. 39, 2018, doi: https://doi.org/10.12989/anr.2018.6.1.039.

[16] D. Akbas Seref, "Bending of a cracked functionally graded nanobeam," (in En), *Advances in nano research*, vol. 6, no. 3, pp. 219–242, 09/25 2018, doi: 10.12989/ANR.2018.6.3.219.

[17] H. Berghouti, E. A. Adda Bedia, A. Benkhedda, and A. Tounsi, "Vibration analysis of nonlocal porous nanobeams made of functionally graded material," (in En), *Advances in nano research*, vol. 7, no. 5, pp. 351–364, 09/25 2019, doi: 10.12989/ANR.2019.7.5.351.

[18] O. Civalek, B. Uzun, and M. O. Yayli, "Frequency, bending and buckling loads of nanobeams with different cross sections," (in En), *Advances in nano research*, vol. 9, no. 2, pp. 91–104, 08/25 2020, doi: 10.12989/ANR.2020.9.2.091.

[19] L. Hadji and M. Avcar, "Nonlocal free vibration analysis of porous FG nanobeams using hyperbolic shear deformation beam theory," (in En), *Advances in nano research*, vol. 10, no. 3, pp. 281–293, 03/25 2021, doi: 10.12989/ANR.2021.10.3.281.

[20] T. Cuong-Le, D. Nguyen Khuong, H. Le-Minh, P. Phan-Vu, P. Nguyen-Trong, and A. Tounsi, "Nonlinear bending analysis of porous sigmoid FGM nanoplate via IGA and nonlocal strain gradient theory," (in En), *Advances in nano research*, vol. 12, no. 5, pp. 441–455, 05/25 2022, doi: 10.12989/ANR.2022.12.5.441.

[21] I. Devnath, N. Islam Mohammad, M. Siddique Minhaj Uddin, and A. Tounsi, "Static deflection of nonlocal Euler Bernoulli and Timoshenko beams by Castigliano's theorem," (in En), *Advances in nano research*, vol. 12, no. 2, pp. 139–150, 02/25 2022, doi: 10.12989/ANR.2022.12.2.139.

[22] A. Saimi, I. Bensaid, and A. Fellah, "Effect of crack presence on the dynamic and buckling responses of bidirectional functionally graded beams based on quasi-3D beam model and differential quadrature finite element method," *Archive of Applied Mechanics*, 2023/05/04 2023, doi: 10.1007/s00419-023-02429-w.

[23] A. Saimi, I. Bensaid, and Ö. Civalek, "A study on the crack presence effect on dynamical behaviour of bi-directional compositionally imperfect material graded micro beams," *Composite Structures*, vol. 316, p. 117032, 2023/07/15/ 2023, doi: https://doi.org/10.1016/j.compstruct.2023.117032.

[24] F. Hadjoui, A. Saimi, I. Bensaid, and A. Hadjoui, "Dynamic analysis of a functionally graded tapered rotating shaft under thermal load via differential quadrature finite elements method," (in En), *Advances in aircraft and spacecraft science*, vol. 10, no. 1, pp. 19–49, 01/25 2023, doi: 10.12989/AAS.2023.10.1.019.

[25] A. Saimi and A. Hadjoui, "An engineering application of the h-p version of the finite elements method to the dynamics analysis of a symmetrical on-board rotor," *European Journal of Computational Mechanics*, vol. 25, no. 5, pp. 388–416, 2016/09/02 2016, doi: 10.1080/17797179.2016.1245597.

[26] N. Wattanasakulpong, B. Gangadhara Prusty, D. W. Kelly, and M. Hoffman, "Free vibration analysis of layered functionally graded beams with experimental validation," *Materials & Design (1980–2015)*, vol. 36, pp. 182–190, 2012/04/01/ 2012, doi: https://doi.org/10.1016/j.matdes.2011.10.049.

[27] N. Wattanasakulpong and V. Ungbhakorn, "Linear and nonlinear vibration analysis of elastically restrained ends FGM beams with porosities," *Aerospace Science and Technology*, vol. 32, no. 1, pp. 111–120, 2014/01/01/ 2014, doi: https://doi.org/10.1016/j.ast.2013.12.002.

[28] M. Jabbari, A. Mojahedin, A. R. Khorshidvand, and M. R. Eslami, "Buckling Analysis of a Functionally Graded Thin Circular Plate Made of Saturated Porous Materials," *Journal of Engineering Mechanics*, vol. 140, no. 2, pp. 287–295, 2014, doi: doi: 10.1061/(ASCE)EM.1943-7889.0000663.

[29] D. Chen, J. Yang, and S. Kitipornchai, "Elastic buckling and static bending of shear deformable functionally graded porous beam," *Composite Structures*, vol. 133, pp. 54–61, 2015/12/01/ 2015, doi: https://doi.org/10.1016/j.compstruct.2015.07.052.

[30] D. Chen, S. Kitipornchai, and J. Yang, "Nonlinear free vibration of shear deformable sandwich beam with a functionally graded porous core," *Thin-Walled Structures*, vol. 107, pp. 39–48, 2016/10/01/ 2016, doi: https://doi.org/10.1016/j.tws.2016.05.025.

[31] A. S. Rezaei and A. R. Saidi, "Application of Carrera Unified Formulation to study the effect of porosity on natural frequencies of thick porous–cellular plates," *Composites Part B: Engineering*, vol. 91, pp. 361–370, 2016/04/15/ 2016, doi: https://doi.org/10.1016/j.compositesb.2015.12.050.

[32] M. R. Barati and A. M. Zenkour, "Investigating post-buckling of geometrically imperfect metal foam nanobeams with symmetric and asymmetric porosity distributions," *Composite Structures*, vol. 182, pp. 91–98, 2017/12/15/ 2017, doi: https://doi.org/10.1016/j.compstruct.2017.09.008.

[33] P. T. Thang, T. Nguyen-Thoi, D. Lee, J. Kang, and J. Lee, "Elastic buckling and free vibration analyses of porous-cellular plates with uniform and non-uniform porosity distributions," *Aerospace Science and Technology*, vol. 79, pp. 278–287, 2018/08/01/ 2018, doi: https://doi.org/10.1016/j.ast.2018.06.010.

[34] F. Ebrahimi and A. Jafari, "A four-variable refined shear-deformation beam theory for thermo-mechanical vibration analysis of temperature-dependent FGM beams with porosities," *Mechanics of Advanced Materials and Structures*, vol. 25, no. 3, pp. 212–224, 2018/02/17 2018, doi: 10.1080/15376494.2016.1255820.

[35] J. S. Stölken and A. G. Evans, "A microbend test method for measuring the plasticity length scale," *Acta Materialia*, vol. 46, no. 14, pp. 5109–5115, 1998/09/01/ 1998, doi: https://doi.org/10.1016/S1359-6454(98)00153-0.

[36] N. A. Fleck, G. M. Muller, M. F. Ashby, and J. W. Hutchinson, "Strain gradient plasticity: Theory and experiment," *Acta Metallurgica*

et Materialia, vol. 42, no. 2, pp. 475–487, 1994/02/01/ 1994, doi: https://doi.org/10.1016/0956-7151(94)90502-9.

[37] C. W. Lim, G. Zhang, and J. N. Reddy, "A higher-order nonlocal elasticity and strain gradient theory and its applications in wave propagation," *Journal of the Mechanics and Physics of Solids*, vol. 78, pp. 298–313, 2015/05/01/ 2015, doi: https://doi.org/10.1016/j.jmps.2015.02.001.

[38] R. D. Mindlin, "Second gradient of strain and surface-tension in linear elasticity," *International Journal of Solids and Structures*, vol. 1, no. 4, pp. 417–438, 1965/11/01/ 1965, doi: https://doi.org/10.1016/0020-7683(65)90006-5.

[39] D. C. C. Lam, F. Yang, A. C. M. Chong, J. Wang, and P. Tong, "Experiments and theory in strain gradient elasticity," *Journal of the Mechanics and Physics of Solids*, vol. 51, no. 8, pp. 1477–1508, 2003/08/01/ 2003, doi: https://doi.org/10.1016/S0022-5096(03)00053-X.

[40] B. Akgöz and Ö. Civalek, "A size-dependent shear deformation beam model based on the strain gradient elasticity theory," *International Journal of Engineering Science*, vol. 70, pp. 1–14, 2013/09/01/ 2013, doi: https://doi.org/10.1016/j.ijengsci.2013.04.004.

[41] M. Mirsalehi, M. Azhari, and H. Amoushahi, "Buckling and free vibration of the FGM thin micro-plate based on the modified strain gradient theory and the spline finite strip method," *European Journal of Mechanics - A/Solids*, vol. 61, pp. 1–13, 2017/01/01/ 2017, doi: https://doi.org/10.1016/j.euromechsol.2016.08.008.

[42] Y. S. Li, W. J. Feng, and Z. Y. Cai, "Bending and free vibration of functionally graded piezoelectric beam based on modified strain gradient theory," *Composite Structures*, vol. 115, pp. 41–50, 2014/08/01/ 2014, doi: https://doi.org/10.1016/j.compstruct.2014.04.005.

[43] S. Thai, H.-T. Thai, T. P. Vo, and V. I. Patel, "Size-dependant behaviour of functionally graded microplates based on the modified strain gradient elasticity theory and isogeometric analysis," *Computers & Structures*, vol. 190, pp. 219–241, 2017/10/01/ 2017, doi: https://doi.org/10.1016/j.compstruc.2017.05.014.

[44] M. Şimşek and J. N. Reddy, "Bending and vibration of functionally graded microbeams using a new higher order beam theory and the modified couple stress theory," *International Journal of Engineering Science*, vol. 64, pp. 37–53, 2013/03/01/ 2013, doi: https://doi.org/10.1016/j.ijengsci.2012.12.002.

[45] L.-L. Ke, Y.-S. Wang, and Z.-D. Wang, "Thermal effect on free vibration and buckling of size-dependent microbeams," *Physica*

E: Low-dimensional Systems and Nanostructures, vol. 43, no. 7, pp. 1387–1393, 2011/05/01/ 2011, doi: https://doi.org/10.1016/j.physe.2011.03.009.

[46] C. M. Wang, S. Kitipornchai, C. W. Lim, and M. Eisenberger, "Beam Bending Solutions Based on Nonlocal Timoshenko Beam Theory," *Journal of Engineering Mechanics*, vol. 134, no. 6, pp. 475–481, 2008, doi: 10.1061/(ASCE)0733-9399(2008)134:6(475).

[47] Y. Q. Wang, H. L. Zhao, C. Ye, and J. W. Zu, "A Porous Microbeam Model for Bending and Vibration Analysis Based on the Sinusoidal Beam Theory and Modified Strain Gradient Theory," *International Journal of Applied Mechanics*, vol. 10, no. 05, p. 1850059, 2018, doi: 10.1142/s175882511850059x.

[48] I. Bensaid and A. Saimi, "Dynamic investigation of functionally graded porous beams resting on viscoelastic foundation using generalised differential quadrature method," *Australian Journal of Mechanical Engineering*, pp. 1–20, 2022, doi: 10.1080/14484846.2021.2017115.

[49] A. Karamanli and M. Aydogdu, "Vibration of functionally graded shear and normal deformable porous microplates via finite element method," *Composite Structures*, vol. 237, p. 111934, 2020/04/01/ 2020, doi: https://doi.org/10.1016/j.compstruct.2020.111934.

[50] X. Huang, H. Hao, K. Oslub, M. Habibi, and A. Tounsi, "Dynamic stability/instability simulation of the rotary size-dependent functionally graded microsystem," *Engineering with Computers,* 2021/05/12 2021, doi: 10.1007/s00366-021-01399-3.

[51] A. Shariati, M. Habibi, A. Tounsi, H. Safarpour, and M. Safa, "Application of exact continuum size-dependent theory for stability and frequency analysis of a curved cantilevered microtubule by considering viscoelastic properties," *Engineering with Computers*, vol. 37, no. 4, pp. 3629–3648, 2021/10/01 2021, doi: 10.1007/s00366-020-01024-9.

[52] S. Ahmed, H. Abdelhamid, B. Ismail, and F. Ahmed, "An Differential Quadrature Finite Element and the Differential Quadrature Hierarchical Finite Element Methods for the Dynamics Analysis of on Board Shaft," *European Journal of Computational Mechanics*, pp. 303–344, 2020, doi: https://doi.org/10.13052/ejcm1779-7179.29461.

[53] C. Liu, B. Liu, L. Zhao, Y. Xing, C. Ma, and H. Li, "A differential quadrature hierarchical finite element method and its applications to vibration and bending of Mindlin plates with curvilinear domains," *International Journal for Numerical Methods in Engineering*, vol. 109, no. 2, pp. 174–197, 2017, doi: https://doi.org/10.1002/nme.5277.

[54] A. A. Abdelrahman, I. Esen, and M. A. Eltaher, "Vibration response of Timoshenko perforated microbeams under accelerating load and thermal environment," *Applied Mathematics and Computation*, vol. 407, p. 126307, 2021/10/15/ 2021, doi: https://doi.org/10.1016/j.amc.2021.126307.

[55] G. Manickam, P. Gupta, S. De, V. Rajamohan, and O. Polit, "Nonlinear flexural free vibrations of size-dependent graphene platelets reinforced curved nano/micro beams by finite element approach coupled with trigonometric shear flexible theory," *Mechanics of Advanced Materials and Structures*, vol. 29, no. 17, pp. 2489–2515, 2022/07/05 2022, doi: 10.1080/15376494.2020.1866723.

[56] M. Liao, "Weak-Form Quadrature Element Method: A Comparative Review of Different Formulations and Its Comprehensive Assessment," *Archives of Computational Methods in Engineering*, 2022/08/17 2022, doi: 10.1007/s11831-022-09799-4.

[57] Y. Tlidji, R. Benferhat, and D. Tahar Hassaine, "Study and analysis of the free vibration for FGM microbeam containing various distribution shape of porosity," (in En), *Structural Engineering and Mechanics*, vol. 77, no. 2, pp. 217–229, 01/25 2021, doi: 10.12989/SEM.2021.77.2.217.

[58] B. Karami, D. Shahsavari, M. Janghorban, and L. Li, "Free vibration analysis of FG nanoplate with poriferous imperfection in hygrothermal environment," *Structural Engineering and Mechanics, An Int'l Journal*, vol. 73, no. 2, pp. 191–207, 2020.

[59] A. Karamanli and M. Aydogdu, "Structural dynamics and stability analysis of 2D-FG microbeams with two-directional porosity distribution and variable material length scale parameter," *Mechanics Based Design of Structures and Machines*, vol. 48, no. 2, pp. 164–191, 2020/03/03 2020, doi: 10.1080/15397734.2019.1627219.

[60] N. Shafiei, S. S. Mirjavadi, B. MohaselAfshari, S. Rabby, and M. Kazemi, "Vibration of two-dimensional imperfect functionally graded (2D-FG) porous nano-/micro-beams," *Computer Methods in Applied Mechanics and Engineering*, vol. 322, pp. 615–632, 2017/08/01/ 2017, doi: https://doi.org/10.1016/j.cma.2017.05.007.

[61] N. Shafiei and M. Kazemi, "Buckling analysis on the bi-dimensional functionally graded porous tapered nano-/micro-scale beams," *Aerospace Science and Technology*, vol. 66, pp. 1–11, 2017/07/01/ 2017, doi: https://doi.org/10.1016/j.ast.2017.02.019.

[62] F. Yang, A. C. M. Chong, D. C. C. Lam, and P. Tong, "Couple stress based strain gradient theory for elasticity," *International Journal of Solids and Structures*, vol. 39, no. 10, pp. 2731–2743, 2002/05/01/ 2002, doi: https://doi.org/10.1016/S0020-7683(02)00152-X.

[63] I. Bensaid, A. Saimi, and Ö. Civalek, "Effect of two-dimensional material distribution on dynamic and buckling responses of graded ceramic-metal higher order beams with stretch effect," *Mechanics of Advanced Materials and Structures*, pp. 1–17, 2022, doi: 10.1080/15376494.2022.2142342.

[64] I. E. Houalef, I. Bensaid, A. Saimi, and A. Cheikh, "Free Vibration Analysis of Functionally Graded Carbon Nanotube-Reinforced Higher Order Refined Composite Beams Using Differential Quadrature Finite Element Method," *European Journal of Computational Mechanics*, vol. 31, no. 04, pp. 505–538, 02/06 2023, doi: 10.13052/ejcm2642-2085.3143.

[65] S. Ahmed, H. Abdelhamid, B. Ismail, and F. Ahmed, "An Differential Quadrature Finite Element and the Differential Quadrature Hierarchical Finite Element Methods for the Dynamics Analysis of on Board Shaft," *European Journal of Computational Mechanics*, vol. 29, no. 4–6, pp. 303–344, 05/13 2021, doi: 10.13052/ejcm1779-7179.29461.

Biographies

Ahmed Saimi obtained his Ph.D in Mechanics of Materials and Structures from the University of Tlemcen, Algeria, in 2017. He is currently a Senior Lecturer at the National High School of Hydraulics Blida, Algeria. A researcher member of Mechanical Systems and Structural Engineering Laboratory, IS2M/UABT. His research interests are: Finite element methods, Structural vibration, Structural dynamics, Dynamics of rotors, Dynamics of rotating machines, computational mechanics, FG materials, Composite materials.

Ismail Bensaid received his B.Sc, M.Sc and Ph.D degrees in Mechanical Engineering from Abou Beckr Belkaid University Tlemcen, Algeria. He is currently working in the level of the Mechanical engineering department at the same University. Dr. Bensaid does research in Mechanical and structural Engineering, Materials, Composite, Maintenance, Nanostructures and Dynamical Systems. He, as an author/co-author, has published more than 18 articles in various journals.

Besma Khouani, Ph.D student in Mechanical Engineering from Abou Beckr Belkaid University Tlemcen, Algeria. He is currently working in the level of the Mechanical engineering department at the same University. Mechanical and structural Engineering, Materials, Composite, Maintenance, Nanostructures and Dynamical Systems.

Med Yassin Mazari, Ph.D student in Mechanical Engineering from Abou Beckr Belkaid University Tlemcen, Algeria. He is currently working in the level of the Mechanical engineering department at the same University. Mechanical and structural Engineering, Materials, Composite, Maintenance, Nanostructures and Dynamical Systems.

Ihab Eddine Houalef, Ph.D student in Mechanical Engineering from Abou Beckr Belkaid University Tlemcen, Algeria. He is currently working in the level of the Mechanical engineering department at the same University. Mechanical and structural Engineering, Materials, Composite, Maintenance, Nanostructures and Dynamical Systems.

Abdelmadjid Cheikh obtained his PhD in production engineering and production management from the University of Nottingham, United Kingdom. He is currently a professor at the University of Tlemcen, Algeria (UABT). He also holds the position of Research Director in Mechanical Systems and Materials Engineering Laboratory (IS2M/UABT). His research interests are: Materials Engineering, Manufacturing Engineering, CAD/CAM, Computer Aided Tolerancing, Rapid Prototyping Processes, CNC Machining, 3D Printing, Optimization.